

An Update of the HLS Estimate of the Muon $g - 2$

M. Benayoun^a, P. David^a, L. DelBuono^a, F. Jegerlehner^{b,c}

^a LPNHE des Universités Paris VI et Paris VII, IN2P3/CNRS, F-75252 Paris, France

^b Humboldt–Universität zu Berlin, Institut für Physik, Newtonstrasse 15, D–12489 Berlin, Germany

^c Deutsches Elektronen–Synchrotron (DESY), Platanenallee 6, D–15738 Zeuthen, Germany

April 4, 2019

Abstract

A global fit of parameters allows us to pin down the Hidden Local Symmetry (HLS) effective Lagrangian, which we apply for the prediction of the leading hadronic vacuum polarization contribution to the muon $g - 2$. The latter is dominated by the annihilation channel $e^+e^- \rightarrow \pi^+\pi^-$, for which data are available by scan (CMD-2 & SND) and ISR (KLOE-2008, KLOE-2010 & BaBar) experiments. It is well known that the different data sets are not in satisfactory agreement. In fact it is possible to fix the model parameters without using the $\pi^+\pi^-$ data, by using instead the dipion spectra measured in the τ -decays together with experimental spectra for the $\pi^0\gamma$, $\eta\gamma$, $\pi^+\pi^-\pi^0$, K^+K^- , $K^0\bar{K}^0$ final states supplemented by specific meson decay properties. Among these, the accepted decay width for $\rho^0 \rightarrow e^+e^-$ and the partial widths and phase information for the $\omega/\phi \rightarrow \pi^+\pi^-$ transitions, are considered. It is then shown that, relying on this global data set, the HLS model, appropriately broken, allows to predict accurately the pion form factor up to 1.05 GeV. It is shown that the data samples provided by CMD-2, SND and KLOE-2010 behave consistently with each other and with the other considered data. Consistency problems with the KLOE-2008 and BaBar data samples are substantiated. "All data" global fits are investigated by applying a reweighting to the conflicting data sets. Constraining to our best fit, the broken HLS model yields $a_\mu^{\text{th}} = (11\,659\,169.55 + \left[\begin{smallmatrix} +1.26 \\ -0.59 \end{smallmatrix} \right]_\phi \pm 5.21_{\text{th}}) 10^{-10}$ associated with a very good global fit probability. Correspondingly, we find that $\Delta a_\mu = a_\mu^{\text{exp}} - a_\mu^{\text{th}}$ exhibits a significance ranging between 4.7 and 4.9 σ .

1 Introduction

The theoretical value for muon anomalous magnetic moment a_μ is an important window in the quest for new phenomena in particle physics. The predicted value is the sum of several contributions and the most prominent ones are already derived from the Standard Model with very high accuracies. The QED contribution is thus estimated with an accuracy of a few 10^{-12} [1, 2, 3] and the precision of the electroweak contribution is now of order 10^{-11} [4]. The light-by-light contribution to a_μ is currently known with an accepted accuracy of 2.6×10^{-10} [5].

Presently, the uncertainty of the Standard Model prediction for a_μ is driven by the uncertainty on the leading order (LO) hadronic vacuum polarization (HVP) up to $\simeq 2$ GeV [6, 7]. This region is covered by the non-perturbative regime of QCD and the leading order HVP ($LO - HVP$) is evaluated by means of :

$$\begin{cases} a_\mu^{LO-HVP} = \sum_i a_\mu(H_i) \\ a_\mu(H_i) = \frac{1}{4\pi^3} \int_{s_{H_i}}^{s_{cut}} ds K(s) \sigma_{H_i}(s) \end{cases} , \quad (1)$$

which relates the hadronic intermediate state contributions $\{H_i, i = 1 \cdots n\}$ to the annihilation cross sections $\sigma(e^+e^- \rightarrow H_i) \equiv \sigma_{H_i}(s)$. $K(s)$ is a known kernel [4] enhancing the weight of the threshold region s_{H_i} and s_{cut} is some energy squared where perturbative QCD starts to be applicable. In the region where perturbative QCD holds¹, its contribution to a_μ carries an uncertainty of the order of a few 10^{-11} .

Up to very recently, the single method used to get the $a_\mu(H_i)$'s was to plug the experimental cross sections into Eq. (1). Among the most recent studies based on this method, let us quote [8, 6, 7, 9]. When several data sets cover the same cross section $\sigma_{H_i}(s)$, Eq. (1) is used with some appropriate weighting of the various spectra, allowing to improve the corresponding $a_\mu(H_i)$.

On the other hand, it is now widely accepted that the Vector Meson Dominance (VMD) concept applies to low energy physics [10, 11]. VMD based Effective Lagrangians have been proposed like the Resonance Chiral Perturbation Theory or the Hidden Local Symmetry (HLS) Model; it was soon proved [12] that these were equivalent. Intrinsically, this means that there exist physics correlations between the various $e^+e^- \rightarrow H_j$ annihilation channels. Therefore, it becomes conceptually founded to expect improving each $a_\mu(H_i)$ by means of the data covering the other channels $e^+e^- \rightarrow H_j$ ($j \neq i$).

This is basically the idea proposed in [13] relying on the HLS model [14, 15]. Using a symmetry breaking mechanism based on the simple BKY idea [16] and a vector meson mixing scheme, the model has been developed stepwise [17, 18, 19, 20] and its most recent form [13] has been shown to provide a successful *simultaneous* description of the e^+e^- annihilation into the $\pi^+\pi^-$, $\pi^0\gamma$, $\eta\gamma$, $\pi^+\pi^-\pi^0$, K^+K^- , $K^0\bar{K}^0$ final states as well as the $\tau^\pm \rightarrow \nu_\tau \pi^\pm \pi^0$ decay spectrum. Some more decays of the form² $V \rightarrow P\gamma$ or $P \rightarrow \gamma\gamma$ are considered.

¹The charmonium and bottomium regions carry uncertainties also in the range of a few 10^{-11} .

²We denote by V or P resp. any meson belonging to the (basic) vector or pseudoscalar lowest mass nonets.

As higher mass meson nonets are absent from the standard HLS model, its energy scope is *a priori* limited upwards by the ϕ meson mass region ($\simeq 1.05$ GeV). However, as this region contributes more than 80 % to the total HVP, improvements which can follow from the broken HLS model are certainly valuable³.

The global simultaneous fit of the data corresponding to the channels quoted above allows to reconstruct the various cross sections $\sigma_{H_i}(s)$ taking automatically into account the physics correlations inside the set $\mathcal{H} \equiv \{H_i\}$ of possible final states and decay processes. The fit parameter values and the parameter error covariance matrix summarize optimally the full knowledge of \mathcal{H} . This has two important consequences :

- One should get the $\{a_\mu(H_i), i = 1, \dots, n\}$ with improved uncertainties by integrating the *model* cross sections instead of the *measured* ones. Indeed, the functional correlations among the various cross sections turn out to provide (much) larger statistics in *each* channel and thus yield improved uncertainties for *each* $a_\mu(H_i)$.
- When several data samples cover the same process H_i , one has a handle to motivatedly examine the behavior of each within the global fit context. Stated otherwise, the issue of the consistency of each data set with *all* the others can be addressed with the (global) fit probability as a tool to detect data samples carrying problematic properties.

Up to now, the broken HLS model (BHLS) [13] – basically an empty shell – has been fed with all existing data sets⁴ for what concerns the annihilation channels $\pi^0\gamma$, $\eta\gamma$, $\pi^+\pi^-\pi^0$, K^+K^- , $K^0\bar{K}^0$, with the spectra from ALEPH [21], CLEO [22] and BELLE [23] for the τ dipion decay⁵ and with the $VP\gamma/P\gamma\gamma$ partial width information extracted from the Review of Particle Properties (RPP) [24]. This already represents more than 40 data sets collected by different groups with different detectors; one may thus consider that the systematics affecting these data sets wash out to a large extent within a global fit framework.

For what concerns the crucial process $e^+e^- \rightarrow \pi^+\pi^-$, the analysis in [13] only deals with the data sets collected in the scan experiments performed at Novosibirsk and referred to globally hereafter as NSK [25, 26, 27, 28, 29]. The main reason was, at this step, to avoid discussing the reported tension [30, 8] between the various existing $\pi^+\pi^-$ data sets : the scan data sets just quoted, and the data sets collected using the Initial State Radiation (ISR) method by KLOE [31, 32] and BaBar [33, 34], not to mention the pion form factor data collected in the spacelike region [35, 36].

It has thus been shown that the global fit excluding the ISR data sets, allows to yield a splendid fit quality; this proves that the whole collection of data sets considered in [13] is self-consistent and may provide a safe reference, *i.e.* a benchmark, to examine the behavior of other data samples.

Using the fit results, the uncertainty on the contribution to a_μ of each of the annihilation channels considered was improved by – at least – a factor of 2, compared to the standard

³The broken HLS model does not include the 4π , 5π , 6π , $\eta\pi\pi$ and $\omega\pi$ annihilation channels. Therefore, the (small) contribution of these missing channels [13] to a_μ should be still evaluated by direct integration of the experimental cross sections; up to the ϕ mass, this amounts to [13] $(1.55 \pm 0.57_{tot}) 10^{-10}$.

⁴The full list of data sets can be found in [19] or [13] together with a critical analysis of their individual behavior.

⁵The energy region used in the fits has been limited to the $[2m_\pi, 1 \text{ GeV}]$ interval where the three data sets are in accord with each other. This should lessen the effect of some systematic effects.

estimation method based on the numerical integration of the measured cross sections. For the case of the $\pi^+\pi^-$ channel, the final uncertainty was even found slightly better than those obtained with the standard method by merging scan and ISR data, *i.e.* a statistics about 4 times larger in the $\pi^+\pi^-$ annihilation channel.

The main purpose of the present study is an update of the work in [13] aiming at confronting all scan (NSK) and ISR (from BaBar and KLOE) – and even spacelike [35, 36] – $\pi^+\pi^-$ data and reexamine the reported issues [30, 8]. The broken HLS model described in [13] happens to provide a tool allowing to compare the behavior of any of these $\pi^+\pi^-$ data sets when confronted with the $\pi^0\gamma$, $\eta\gamma$, $\pi^+\pi^-\pi^0$, K^+K^- , $K^0\bar{K}^0$ annihilation data *and* with the τ dipion spectra. Indeed, these data alone, supplemented with some limited information extracted from the Review of Particle Properties⁶ (RPP) [24], allow to predict the pion form factor with a surprisingly good precision. The additional RPP information is supposed to carry the Isospin Breaking (IB) information requested in order to derive reliably the $\pi^+\pi^-$ information from the knowledge of the $\pi^\pm\pi^0$ spectrum.

We also take profit of the present work to update the numerical values for some contributions to the muon anomalous moment a_μ , all gathered in Table 10 of [13]. Thus, we update the QED entry by using the recent spectacular progress by Aoyama, Hayakawa, Kinoshita and Nio [1, 2]. They have been able to perform a complete numerical calculation of the 5-loop QED corrections to a_e and a_μ . On the other hand, the electroweak contribution, which depends on the Higgs mass at 2-loops is now better known if we accept that ATLAS [37] and CMS [38] have observed at the LHC the Higgs boson at a mass of about 125 GeV in a narrow window. Using this information slightly changes the central value as well as the uncertainty of the EW entry. We also have reevaluated the higher order HVP contribution (HO) within the standard approach based on all $\pi^+\pi^-$ channels (*i.e.* all scan and ISR data).

The paper is organized as follows. Section 2 reminds (from [13]) a few basic topics concerning the $\pi\pi$ channel description within the BHLS model. In Section 3, the detailed framework – named “ τ +PDG” – used to study the differential behavior of the scan and ISR data is presented. Thanks to the (wider than usual) energy range covered by the BaBar spectrum [33, 34], a detailed study of the $\pi^+\pi^-$ spectrum in the ϕ region can be performed for the first time. This leads to update the $\phi \rightarrow \pi^+\pi^-$ treatment within our computer code; this is emphasized in Subsection 3.3. In Section 4, one confronts the “ τ +PDG” predictions with the available scan (NSK) and ISR data samples; it is shown that the NSK data and both KLOE data samples (referred to hereafter as KLOE08 [31] and KLOE10 [32]) have similar properties while BaBar behaves differently, especially in the $\rho - \omega$ interference region. Section 5 reports on the global fits performed using the various $\pi^+\pi^-$ data samples each in isolation or combined. Subsection 5.1.4 is devoted to studying the ϕ region of the pion form factor. In Section 6, we focus on the consequences for the muon anomalous moment a_μ of the various scan and ISR $\pi^+\pi^-$ spectra and compare results with the BNL [39, 40] measurement. The $\pi^+\pi^-$ intermediate state contribution to a_μ from the invariant mass region [0.630, 0.958] GeV is especially considered as it serves to examine the outcome of various fits with respect to the experimental expectations. Finally, Section 7 is devoted to conclusions.

⁶We occasionally refer to the RPP as Particle Data Group (PDG).

2 A Brief Reminder Of Concern for the $\pi\pi$ Channel

2.1 The Broken HLS Lagrangian

The general framework of our analysis is the resonance Lagrangian extension [10, 12] of Chiral Perturbation Theory (ChPT), the latter being the systematic and unambiguous approach to low energy effective QCD [41, 42]. This approach can also be viewed as an attempt to implement the VMD model in a way consistent with the chiral structure of QCD. Like in ChPT, the basic fields are the unitary matrix fields $\xi_{L,R} = \exp [\pm i P/f_\pi]$, where $P = P_8 + P_0$ is the $SU(3)$ matrix of pseudoscalar fields, with P_0 and P_8 being respectively the basic singlet and octet field matrices. The Hidden Local Symmetry (HLS) ansatz [14, 15] is an extension of the ChPT non-linear sigma model to a non-linear chiral Lagrangian based on the symmetry pattern $G_{\text{global}}/H_{\text{local}}$, where $G = SU(3)_L \otimes SU(3)_R$ is the chiral group of QCD and $H = SU(3)_V$ is the vector subgroup. The hidden local $SU(3)_V$ requires the spin 1 vector meson fields, represented by the $SU(3)$ matrix field V_μ , to be gauge fields. The corresponding covariant derivative reads $D_\mu = \partial_\mu - i g V_\mu$ and can be naturally extended [15] in order to include the couplings to the electroweak gauge fields A_μ , Z_μ and W_μ^\pm . As the coupling to the Z boson is not relevant in our context, it is omitted in the following. The unbroken HLS Lagrangian is then given by $\mathcal{L}_{\text{HLS}} = \mathcal{L}_A + a\mathcal{L}_V$, where

$$\mathcal{L}_{A/V} = -\frac{f_\pi^2}{4} \text{Tr} [L \pm R]^2, \quad (2)$$

with $L = [D_\mu \xi_L] \xi_L^\dagger$ and $R = [D_\mu \xi_R] \xi_R^\dagger$; a is a basic HLS parameter not fixed by the theory which should be derived from data. From standard VMD models, one expects $a \simeq 2$.

In fact the global chiral symmetry G_{global} is well known not to be realized as an exact symmetry in nature which implies that the ideal HLS symmetry is evidently not a symmetry of nature either. Therefore, it has obviously to be broken appropriately in order to provide a realistic low energy effective theory mimicking low energy effective QCD.

Unlike in ChPT where one is performing a systematic low energy expansion in low momenta and the quark masses, here one introduces symmetry breaking as phenomenological parameters to be fixed from appropriate data. Indeed, a systematic low energy expansion à la ChPT ceases to converge at energies above $\simeq 400$ MeV, while we attempt to model phenomenology up to, and including, the ϕ resonance region.

In our approach, the Lagrangian pieces in Eqs (2) undergo a first breaking mechanism named BKY, originally defined in [16]. It has been reformulated in [17] in order to avoid some undesirable properties. In its original form, this BKY breaking scheme covers only the breaking of the $SU(3)$ symmetry; following [43], the BKY breaking has been extended in order to include isospin symmetry breaking effects. This turns out to modify Eqs. (2) by introducing two constant diagonal matrices $X_{A/V}$:

$$\mathcal{L}_{A/V} \implies \mathcal{L}'_{A/V} = -\frac{f_\pi^2}{4} \text{Tr} \{ [L \pm R] X_{A/V} \}^2 \quad (3)$$

and the (non-zero) entries in $X_{A/V}$ are fixed from fit to the data. The final broken HLS Lagrangian can be written :

$$\mathcal{L}'_{\text{HLS}} = \mathcal{L}'_A + a\mathcal{L}'_V + \mathcal{L}_{\text{thooft}}, \quad (4)$$

where \mathcal{L}'_{tHooft} contains determinant terms [44] breaking the nonet symmetry in the pseudoscalar sector. \mathcal{L}'_{HLS} can be found expanded in [13].

However, in order to account successfully for the largest possible set of data, isospin symmetry breaking should be completed by the kaon loop mixing of the neutral vector mesons (ρ_I^0 , ω_I and ϕ_I). This implies a change of fields to be performed in the \mathcal{L}'_{HLS} Lagrangian. This mixing mechanism is briefly reminded just below.

2.2 Mixing of Neutral Vector Mesons Through Kaon Loops

It has been shown [19, 20, 13] that \mathcal{L}'_{HLS} is insufficient in order to get a good simultaneous account of the $e^+e^- \rightarrow \pi^+\pi^-$ annihilation data and of the dipion spectrum in the $\tau^\pm \rightarrow \nu_\tau \pi^\pm \pi^0$ decay. A consistent solution to this problem is provided by the vector field mixing mechanism first introduced in [18].

Basically, the vector field mixing is motivated by the one-loop corrections to the vector field squared mass matrix. These are generated by the following term of the broken HLS Lagrangian⁷ \mathcal{L}'_{HLS} :

$$\frac{ia_g}{4z_A} \left\{ [\rho_I^0 + \omega_I - \sqrt{2}z_V \phi_I] K^- \overset{\leftrightarrow}{\partial} K^+ + [\rho_I^0 - \omega_I + \sqrt{2}z_V \phi_I] K^0 \overset{\leftrightarrow}{\partial} \bar{K}^0 \right\}, \quad (5)$$

where g is the universal vector coupling and the subscript I indicates ideal vector fields.

Therefore, the vector meson squared mass matrix M_0^2 , which is diagonal at tree level, undergoes corrections at one-loop. The perturbation matrix $\delta M^2(s)$ [18, 19, 20] depends on the square of the momentum flowing through the vector meson lines. The diagonal entries acquire self-mass corrections – noticeably the ρ^0 entry absorbs the pion loop – but non-diagonal entries appear and correspond to transitions among the ideal ρ^0 , ω and ϕ meson fields which originally enter the HLS Lagrangian : $\Pi_{\omega\phi}(s)$, $\Pi_{\rho\omega}(s)$ and $\Pi_{\rho\phi}(s)$. These are linear combinations of the neutral and charged kaon loops⁸.

Therefore, at one-loop order, the ideal vector fields which enter \mathcal{L}'_{HLS} are no longer mass eigenstates; the *physical* vector fields are then (re)defined as the eigenvectors of $M^2 = M_0^2 + \delta M^2(s)$. This change of fields should be propagated into the whole broken HLS Lagrangian \mathcal{L}'_{HLS} , extended in order to include the anomalous couplings [45] as done in [13]. For brevity, this Lagrangian is referred to as BHLS.

2.3 The $V\pi\pi$ and $V - \gamma/W^\pm$ Couplings

As the present study focuses on $e^+e^- \rightarrow \pi^+\pi^-$ data, it is worth to briefly remind a few relevant pieces of the \mathcal{L}'_{HLS} Lagrangian. In terms of *physical* vector fields, *i.e.* the eigenstates

⁷ For clarity, we have dropped out the isospin breaking corrections generated by the BKY mechanism; the exact formula can be found in the Appendix A of [13]. The parameter z_V corresponds to breaking of the SU(3) symmetry in the Lagrangian piece \mathcal{L}_V , while z_A is associated with the SU(3) breaking of \mathcal{L}_A . z_V has no really intuitive value, while z_A can be expressed in terms of the kaon and pion decay constants as $z_A = [f_K/f_\pi]^2$.

⁸ Other contributions, like K^*K loops, take place [18, 19] which are essentially real in the energy region up to the ϕ meson mass. These can be considered as numerically absorbed by the subtraction polynomials of the kaon loops.

of $M^2 = M_0^2 + \delta M^2(s)$, the $V\pi\pi$ Lagrangian piece writes :

$$\frac{ia g}{2}(1+\Sigma_V) \left[\left\{ \rho^0 + [(1-h_V)\Delta_V - \alpha(s)] \omega + \beta(s) \phi \right\} \cdot \pi^- \overleftrightarrow{\partial} \pi^+ + \left\{ \rho^- \cdot \pi^+ \overleftrightarrow{\partial} \pi^0 - \rho^+ \cdot \pi^- \overleftrightarrow{\partial} \pi^0 \right\} \right]. \quad (6)$$

Σ_V and $(1-h_V)\Delta_V$ are isospin breaking parameters generated by the BKY mechanism [13], whereas $\alpha(s)$ and $\beta(s)$ are (complex) "angles" which define the physical neutral meson vector fields in terms of their ideal partners. Their expressions can be found in [13].

Another Lagrangian piece relevant for the present update is :

$$- e \left[f_{\rho\gamma}(s)\rho^0 + f_{\omega\gamma}(s)\omega - f_{\phi\gamma}(s)\phi \right] \cdot A - \frac{g_2 V_{ud}}{2} f_{\rho W} \left[W^+ \cdot \rho^- + W^- \cdot \rho^+ \right], \quad (7)$$

where g_2 is the weak coupling constant related with the Fermi constant [15] and V_{ud} is the element of the (u, d) entry in the CKM matrix. The $f_{V\gamma}(s)$ functions and $f_{\rho W}$ are the transition amplitudes of the physical vector mesons to resp. a photon and the W boson. At leading order in the breaking parameters, they are given by [13] :

$$\begin{cases} f_{\rho\gamma}(s) = agf_\pi^2 \left[1 + \Sigma_V + h_V \frac{\Delta_V}{3} + \frac{\alpha(s)}{3} + \frac{\sqrt{2}z_V}{3}\beta(s) \right], \\ f_{\omega\gamma}(s) = \frac{agf_\pi^2}{3} \left[1 + \Sigma_V + 3(1-h_V)\Delta_V - 3\alpha(s) + \sqrt{2}z_V \gamma(s) \right], \\ f_{\phi\gamma}(s) = \frac{agf_\pi^2}{3} \left[-\sqrt{2}z_V + 3\beta(s) + \gamma(s) \right], \\ f_{\rho W} \equiv f_\rho^\tau = agf_\pi^2 [1 + \Sigma_V]. \end{cases} \quad (8)$$

Eqs. (6) and (8) exhibit an important property which should be noted. The functions providing the coupling of the physical ω and ϕ mesons to a pion pair also come into $f_{\rho\gamma}(s)$. Therefore, any change in the conditions used in order to account for the decays $\omega/\phi \rightarrow \pi^-\pi^+$ correspondingly affects the whole description of the $e^+e^- \rightarrow \pi^+\pi^-$ cross section.

2.4 The Pion Form Factor

We only remind the pion form factor in τ decay and in e^+e^- annihilation and refer the interested reader to [13] for detailed information. The pion form factor in the τ^\pm decay to $\pi^\pm\pi^0\nu_\tau$ can be written :

$$F_\pi^\tau(s) = \left[1 - \frac{a}{2}(1 + \Sigma_V) \right] - \frac{ag}{2}(1 + \Sigma_V) F_\rho^\tau(s) \frac{1}{D_\rho(s)}, \quad (9)$$

where a and g are the basic HLS parameters [15] already encountered; Σ_V is one of the isospin breaking parameters introduced by the (extended) BKY breaking scheme. The other quantities are :

$$\begin{cases} F_\rho^\tau(s) = f_\rho^\tau - \Pi_W(s), \\ D_\rho(s) = s - m_\rho^2 - \Pi'_{\rho\rho}(s), \\ f_\rho^\tau = agf_\pi^2(1 + \Sigma_V) \quad , \quad m_\rho^2 = ag^2f_\pi^2(1 + \Sigma_V), \end{cases} \quad (10)$$

where $\Pi_W(s)$ and $\Pi'_{\rho\rho}(s)$ are, respectively, the loop correction to the $\rho^\pm - W^\pm$ transition amplitude and the charged ρ self-mass (see [13]).

The pion form factor in e^+e^- annihilation is more complicated and writes :

$$F_\pi^e(s) = \left[1 - \frac{a}{2}(1 + \Sigma_V + \frac{h_V \Delta_V}{3}) \right] - F_{\rho\gamma}^e(s) \frac{g_{\rho\pi\pi}}{D_\rho(s)} - F_{\omega\gamma}^e(s) \frac{g_{\omega\pi\pi}}{D_\omega(s)} - F_{\phi\gamma}^e(s) \frac{g_{\phi\pi\pi}}{D_\phi(s)}, \quad (11)$$

where $g_{\rho\pi\pi}$, $g_{\omega\pi\pi}$ and $g_{\phi\pi\pi}$ can be read off Eq. (6) and the $F_{V\gamma}^e$ are given by :

$$F_{V\gamma}^e(s) = f_{V\gamma}(s) - \Pi_{V\gamma}(s), \quad (V = \rho_R^0, \omega_R, \phi_R), \quad (12)$$

with the $f_{V\gamma}(s)$ given by Eqs. (8) above and the $\Pi_{V\gamma}(s)$ being loop corrections [13]. $D_\rho(s) = s - m_\rho^2 - \Pi_{\rho\rho}(s)$ is the inverse ρ^0 propagator while $D_\omega(s)$ and $D_\phi(s)$ are the modified fixed width Breit-Wigner functions defined in [13].

3 Confronting the Various $e^+e^- \rightarrow \pi^+\pi^-$ Data Sets

3.1 The Issue

Although the BHLS Lagrangian should be able to describe more complicated hadron production processes, in a first step one obviously has to focus on low multiplicity states, primarily two particle production but also the simplest three particle production channel $e^+e^- \rightarrow \pi^+\pi^-\pi^0$. Four pion production, annihilation to $KK\pi \dots$ are beyond the scope of the basic setup of the BHLS model. We expect that available data on the lowest multiplicity channels provide a consistent database which allows us to pin down all relevant parameters, such that our effective resonance Lagrangian is able to *simultaneously* fit all possible low multiplicity channels. In fact, what is considered are essentially all relevant annihilation channels up to the ϕ ; in this energy range, as already stated, the missing channels ($4\pi, 5\pi, 6\pi, \eta\pi\pi, \omega\pi$) contribute less than 0.3% to a_μ^{had} .

Our previous study [13] has actually shown that the following groups of complementary data samples and/or RPP [24] accepted particle properties (mainly complementary branching fractions) support our global fit strategy :

- **(i)** All e^+e^- annihilation data into the $\pi^0\gamma, \eta\gamma, \pi^+\pi^-\pi^0, K^+K^-, K^0\bar{K}^0$ final states admit a consistent simultaneous fit⁹,
- **(ii)** The $\tau^\pm \rightarrow \nu_\tau \pi^\pm \pi^0$ dipion spectra produced by ALEPH [21], CLEO [22] and BELLE [23], however limited to the energy region where they are in reasonable accord with each other ($\sqrt{s} \leq 1 \text{ GeV}$),
- **(iii)** Some additional partial width from the $P\gamma\gamma$ and $VP\gamma$ decays, which are independent of the annihilation channels listed just above,

⁹ With – possibly – some minor tension between the $\pi^+\pi^-\pi^0$ data around the ϕ resonance and the dikaon data (see the discussions in [19, 13]).

- (iv) Some information concerning the $\phi \rightarrow \pi^-\pi^+$ decay, especially its accepted partial width $\Gamma(\phi \rightarrow \pi^-\pi^+)$ [24]. This piece of information is supposed to partly counterbalance the lack of spectrum for the $e^+e^- \rightarrow \pi^+\pi^-$ annihilation in the ϕ mass region¹⁰.
- (v) All the $e^+e^- \rightarrow \pi^+\pi^-$ data sets (NSK) collected¹¹ by the scan experiments mounted at Novosibirsk, especially CMD-2 [26, 27, 28] and SND [29].

They represent a complete reference collection of data samples and lead to fits which do not exhibit any visible tension between the BHLS model parametrization and the data (see for instance Table 3 in [13]). This is worth being noted, as we are dealing with a large number of different data sets collected by different groups using different detectors and different accelerators. The (statistical & systematic) error covariance matrices used within our fit procedure are cautiously constructed following closely the group claims and recommendations. Therefore, the study in [13] leads to think that the *model* correlations exhibited by BHLS reflect reasonably well the *physics* correlations expected to exist between the various channels.

However, beside the (NSK) $e^+e^- \rightarrow \pi^+\pi^-$ data sets collected in scan mode, there exists now data sets collected using the Initial State Radiation (ISR) method by the KLOE and BaBar Collaborations. All recent studies (see [30, 8], for instance) report upon some "tension" between them. As this issue has important consequences concerning the estimate of the muon anomalous magnetic moment, it is worth examining if the origin of this tension can be identified and, possibly, substantiated. Besides scan and ISR data, it is also interesting to reexamine [18] the pion form factor data collected in the spacelike region [35, 36] within the BHLS framework; indeed, if valid, these data provide strong constraints on the threshold behavior of the pion form factor and, therefore, an improved information on the muon $g - 2$.

3.2 The Analysis Method

The BHLS model has many parameters and a global fit has to be guided by fitting those parameters to those channels to which they are the most sensitive. Obviously resonance parameters of a given resonance have to be derived from a fit of the corresponding invariant mass region. Similarly, the anomalous type interaction responsible for $\pi^0 \rightarrow \gamma\gamma$ or the $\pi\pi\pi$ final state ... are sensitive to very specific channels only.

We also have to distinguish the gross features of the HLS model and the chiral symmetry breaking imposed to it. With this in mind, in our approach, the τ decay spectra play a key role since the charged channel is much simpler than the neutral one where γ , ρ^0 , ω and ϕ are entangled by substantial mixing of the amplitudes, which are not directly observable. In the low energy region, below the kaon pair thresholds and the ϕ region, what comes into play is the ρ^\pm form factor obtained from the τ spectra. Together with the isospin breaking due to $\rho^0 - \omega$ mixing – characterized by the branching fractions $Br(\omega \rightarrow \pi^+\pi^-)$ and $Br(\omega \rightarrow e^+e^-)$, which in a first step can be taken from the RPP – the ρ^\pm form factor should yield a good prediction for the $e^+e^- \rightarrow \pi^+\pi^-$ channel. Data from the latter can then be used to refine the global fit. This will be our strategy in the following.

¹⁰The BaBar data [33] allow, for the first time, to make a motivated statement concerning how this piece of information should be dealt with inside the minimization code. This is discussed below.

¹¹ The data sets [25] collected by former detectors at Novosibirsk are also considered.

The annihilation channels referred to as **(i)** in the above Subsection as well as the decay information listed in **(iii)** have little to do with the $e^+e^- \rightarrow \pi^+\pi^-$ annihilation channels, except for the physics correlations implied by the BHLS model. On the other hand, as long as one limits oneself to the region $(2m_\pi, 1 \text{ GeV})$, there is no noticeable contradiction between the various dipion spectra extracted from the $\tau^\pm \rightarrow \nu_\tau \pi^\pm \pi^0$ decay by the various groups [21, 22, 23]. Therefore, it is motivated to examine the behavior of each of the collected $e^+e^- \rightarrow \pi^+\pi^-$ data sets in isolation while keeping as reference the data corresponding to the channels listed in **(i) – (iii)**. Stated otherwise, the data for the channels listed in **(i) – (iii)**, together with the BHLS model, represent a benchmark, able to examine critically any $e^+e^- \rightarrow \pi^+\pi^-$ data sample.

On the other hand, the Isospin Breaking (IB) effects affecting the dipion spectra from τ decay are independent of those in the $e^+e^- \rightarrow \pi^+\pi^-$ annihilation and can easily be factored out. Therefore, it remains only to account for isospin breaking effects specific of the $e^+e^- \rightarrow \pi^+\pi^-$ channel, in a clearly identified way.

A priori, IB effects specific of the $e^+e^- \rightarrow \pi^+\pi^-$ annihilation are threefold and cover :

- **(j)** Information on the decay $\rho^0 \rightarrow e^+e^-$,
- **(jj)** Information on the decay $\omega \rightarrow \pi^+\pi^-$,
- **(jjj)** Information on the decay $\phi \rightarrow \pi^+\pi^-$.

The importance of decay information on $\rho^0 \rightarrow e^+e^-$ to determine IB effects has been emphasized in only a few previous works [7, 20, 13]. Within the BHLS model, the ratio $f_{\rho\gamma}(s)/f_{\rho W}$ exhibits non-negligible IB effects for this particular coupling (see Fig. 11 in [13]). They amount to several percents in a (threshold) region quite important for evaluating $g - 2$.

There is certainly no piece of information in the data covered by the channels listed in **(i) – (iii)** above concerning the decay information **(jj)** or **(jjj)**. In contrast, the vertex $\rho^0 e^+e^-$ is certainly involved in all the annihilation channels considered. Imposing the RPP [24] information $\Gamma(\rho^0 \rightarrow e^+e^-) = 7.04 \pm 0.06 \text{ keV}$ is, nevertheless, legitimate because the channels **(i) – (iii)** do not significantly constrain the decay width $\rho^0 \rightarrow e^+e^-$.

For the following discussion we define the branching ratio products $F_\omega \doteq \text{Br}(\omega \rightarrow e^+e^-) \times \text{Br}(\omega \rightarrow \pi^+\pi^-)$ and $F_\phi \doteq \text{Br}(\phi \rightarrow e^+e^-) \times \text{Br}(\phi \rightarrow \pi^+\pi^-)$, which are relevant for the prediction of the $e^+e^- \rightarrow \pi^+\pi^-$ channel.

Two alternative analysis strategies can be followed :

- **(k)** Use the so-called accepted values for the $\rho^0 \rightarrow e^+e^-$, $\omega \rightarrow \pi^+\pi^-$ and $\phi \rightarrow \pi^+\pi^-$ as reported in the Review of Particle Properties (RPP). These are the least experiment dependent pieces of information¹². Actually, as argued in [19] (see Subsection 13.3 therein), we prefer using the RPP information for the products $F_\omega = (1.225 \pm 0.071) 10^{-6}$ and $F_\phi = (2.2 \pm 0.4) 10^{-8}$.

We will be even more constraining by supplementing these ω and ϕ branching ratios

¹²Nevertheless, one should keep in mind that these accepted values are highly influenced by the $e^+e^- \rightarrow \pi^+\pi^-$ scan data samples compared to others. Therefore, this choice could favor the CMD-2 and SND data samples within fit procedures; however, as these accepted values are certainly not influenced by none of the BaBar or KLOE data samples, the behavior of each of the various ISR data samples becomes a crucial piece of information.

by phase information : The so-called Orsay phase concerning the ω decay¹³ and the reported phase¹⁴ of the $\phi \rightarrow \pi^+\pi^-$ amplitude relative to $\rho^0 \rightarrow \pi^+\pi^-$.

- **(kk)** Use directly data when possible. Indeed, all relevant IB information carried by $\rho^0 \rightarrow e^+e^-$ and $\omega \rightarrow \pi^+\pi^-$ can be derived within the BHLS model by the difference between the $\pi^+\pi^-$ spectra and the dipion spectrum $\pi^\pm\pi^0$ in the τ decay; more precisely using the $\pi^+\pi^-$ spectrum within the tiny energy region $0.76 \div 0.82$ GeV allows to derive the relevant IB pieces of information in full consistency with our model.

As all scan (NSK) $e^+e^- \rightarrow \pi^+\pi^-$ data samples [25, 26, 27, 28, 29] and both KLOE data sets (KLOE08 and KLOE10) stop below 1 GeV, the ϕ information should be taken from somewhere else, namely from the RPP. Fortunately, the ϕ region is now covered by the BaBar data set [33, 34]. Therefore, as soon as the consistency of the $\phi \rightarrow \pi^+\pi^-$ information carried by the BaBar data and by [24, 48] is established, this part of the spectrum could supplement the scan and KLOE data sets¹⁵.

Concerning the $\phi \rightarrow \pi^+\pi^-$ information, this second strategy will be used by either taking the [24, 48] information or the BaBar data points between 1.0 and 1.05 GeV.

3.3 How to Implement $\omega/\phi \rightarrow \pi^+\pi^-$ PDG Information?

The vector meson couplings to $\pi^+\pi^-$ or e^+e^- depend on the s -dependent "mixing angles" $\alpha(s)$, $\beta(s)$ and $\gamma(s)$. This does not give rise to any ambiguity as long as one deals with spectra; however, when using the PDG information for vector meson decays, especially to $\pi^+\pi^-$ or e^+e^- , one has to specify at which value for s each of the vector meson (model) coupling should be evaluated.

Within the HLS model, there are *a priori* two legitimate choices for the mass of vector mesons; this can either be the Higgs–Kibble (HK) mass which occurs in the Lagrangian after symmetry breaking or, especially for the ω and ϕ mesons, the experimental (accepted) mass as given in the RPP. Prior to the availability of the BaBar data [33], the published $e^+e^- \rightarrow \pi^+\pi^-$ cross section data did not include the ϕ mass region and, therefore, there was no criterion to check the quality of each possible choice in the ϕ mass region¹⁶. The choice made in the previous studies using the broken HLS model [18, 19, 20, 13] was the ϕ HK mass.

If one feeds the broken HLS model with the data listed in **i–iv** (see Subsection 3.1 above), one can make predictions for the pion form factor independently of the measured $e^+e^- \rightarrow \pi^+\pi^-$ data. This procedure is discussed in detail in the next section. Here we anticipate some results specific to the ϕ mass issue.

Fig. (1a) displays the prediction for the pion form factor in the ϕ region using the HK mass to estimate the $\phi\pi^-\pi^+$ coupling constant with the BaBar data superimposed (not fitted); it is clear that the prediction is quite reasonable up to $\simeq 0.98$ GeV as well as above $\simeq 1.05$ GeV.

¹³We will use as input the value $104.7^\circ \pm 4.1^\circ$ found by [46], which is consistent with the results recently derived [47] while using an analogous (HLS) model (see Tables VI–IX therein).

¹⁴The single existing measurement $-34^\circ \pm 4^\circ$ is reported by the SND Collaboration [48].

¹⁵ Actually, the few BaBar data points between, say, 1.0 and 1.05 GeV carry obviously more information than the branching ratio and the "Orsay" phase at the ϕ mass.

¹⁶As the HK mass for the ω meson coincides almost exactly with its accepted RPP value, the problem actually arises only for the ϕ meson.

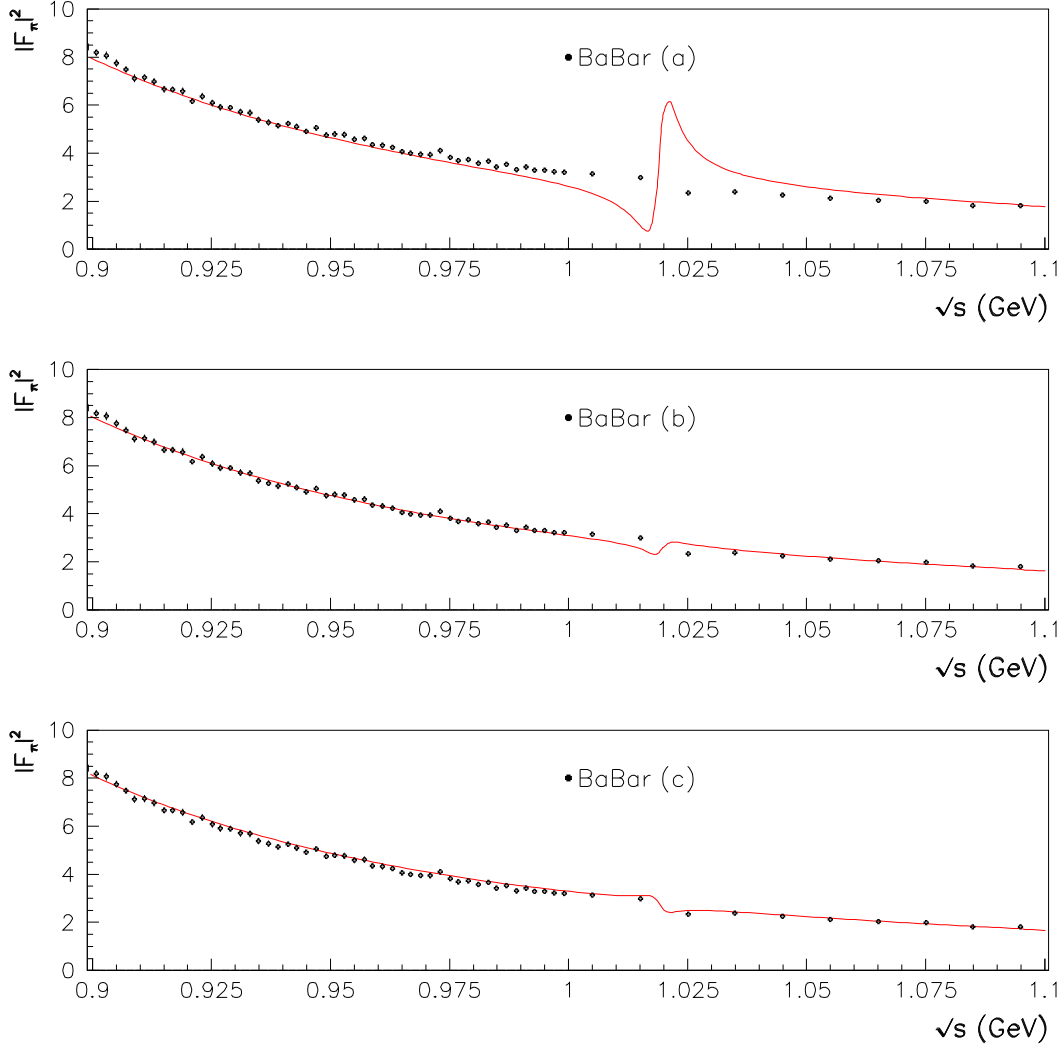


Figure 1: The $e^+e^- \rightarrow \pi^+\pi^-$ cross section around the ϕ mass together with BaBar data. The curve in (a) displays the prediction using the RPP ϕ decay information computed at the ϕ Higgs–Kibble mass; the curve in (b) displays the prediction using the PDG ϕ decay information computed at the experimental ϕ mass. In (c) the PDG ϕ decay information is replaced by the five BaBar data points located between 1. and 1.05 GeV.

However, it is clearly unacceptable for the mass region in-between. In contrast, using the ϕ mass as given in the RPP to extract the $\phi\pi^-\pi^+$ coupling constant from its accepted partial width [24] provides the spectrum shown in Fig. (1b); this alternate choice is certainly reasonable all along the mass region displayed. Therefore, it is motivated to update our former results [13] by

performing the change just emphasized¹⁷.

In order to be complete, it is worth mentioning here a fit result obtained by exchanging the PDG/SND ϕ decay information with the BaBar pion form factor data¹⁵ in the range $(1.0 \div 1.05)$ GeV. The result, given in Fig. (1c), shows that the lineshape of the BaBar pion form factor at the ϕ mass can be satisfactorily accommodated.

4 τ Predictions of the Pion Form Factor

4.1 τ +PDG Predictions

As mentioned before, the charged isovector $\tau^\pm \rightarrow \nu_\tau \pi^\pm \pi^0$ dipion spectra are not affected by $\gamma - \rho - \omega - \phi$ mixing and hence are of much simpler structure. Supplemented by the basic $\rho - \omega - \phi$ mixing effects which derive from $SU(2)$ and $SU(3)$ flavor breaking, one has a good starting point to fix the parameters of the BHLS model to predict the process $e^+e^- \rightarrow \pi^+\pi^-$. Specifically, we are using the data including the channels listed in **i-iv** of Section 3 together with RPP information relevant to fix the IB effects affecting the pion form factor. This method is named, somewhat abusively¹⁸ τ +PDG.

Specifically, the IB effects encoded in $F_\omega \doteq \text{Br}(\omega \rightarrow e^+e^-) \times \text{Br}(\omega \rightarrow \pi^+\pi^-)$ and $F_\phi \doteq \text{Br}(\phi \rightarrow e^+e^-) \times \text{Br}(\phi \rightarrow \pi^+\pi^-)$, are taken from the RPP (and reminded in Subsection 3.2). For the missing phase information we adopt the result from the fit [46] for the Orsay phase of the $\omega \rightarrow \pi^+\pi^-$ amplitude and the result from SND [48] for the phase of the $\phi \rightarrow \pi^+\pi^-$ amplitude¹⁹. Following the discussion in the preceding Subsection, the model branching ratios and phases are computed at the vector boson masses accepted by the RPP.

The fit returns a probability of 89.4% with $\chi^2/n_{dof} = 553.4/596$. The fit quality (χ^2/n_{points}) for each of the fitted channels is almost identical to our results in [13] (see the last column in Table 3 therein). Each of the PDG information listed above contributes by $\simeq 1$ to the total χ^2 . It is also worth mentioning that the dipion spectra from [21, 22, 23] are nicely described up to $\sqrt{s} = 1$ GeV and provide residual distributions indistinguishable from those shown in Figure 10 of [13]. From this fit, one derives the (τ +PDG) predictions for the pion form factor which can be compared with the various existing $e^+e^- \rightarrow \pi^+\pi^-$ data samples.

The overall view of the comparison is shown in Fig. 2. This clearly indicates that the data associated with the channels listed in **i-iv**, supplemented with a limited PDG information is indeed able to provide already a satisfactory picture of the pion form factor as reported by all experiments having published $e^+e^- \rightarrow \pi^+\pi^-$ spectra.

Let us stress that the predicted pion form factor relies on the $\pi^\pm\pi^0$ spectra provided by ALEPH [21], Belle [23] and CLEO [22] only up to 1.0 GeV. Therefore, the inset in Fig. 2 actually shows the *extrapolation* of the prediction into the spacelike region with the NA7 data [35] superimposed; this clearly indicates that there is no reason to discard the spacelike data from our data handling. One should also note that the extrapolation of the prediction above the

¹⁷We show later on that choosing the ϕ HK mass has produced some overestimate of the prediction for a_μ and, thus, some underestimate of the discrepancy with the BNL measurement [39, 40].

¹⁸The "Orsay" phase for both the ω and ϕ mesons have no entry in the RPP.

¹⁹A preliminary version of the present work was presented [49] at the Workshop on Meson Transition Form Factors held on May 29-30, 2012 in Krakow, Poland. Some minor differences may occur with the present results due to the fact that the SND phase for $\phi \rightarrow \pi^+\pi^-$ was not imposed in the preliminary work.

ϕ mass is quite reasonable up to $\simeq 1.2 \div 1.3$ GeV. This may indicate that the influence of high mass vector mesons is negligible up to this energy region.

In order to make more precise statements, let us magnify piece wise the information carried by Fig. 2. Thus, Fig. 3 displays the behavior of the various $e^+e^- \rightarrow \pi^+\pi^-$ data samples in the $(0.3 \div 0.7)$ GeV energy region. As a general statement the behavior expected from the existing data samples looks well predicted by the τ +PDG method. A closer inspection allows to infer that the CMD-2 and SND data points (*i.e.* NSK when used together) are well spread onto both sides of the predicted curve; this property is also shared by the KLOE10 sample. Even if reasonably well described, the KLOE08 and BaBar data samples are lying marginally above the τ +PDG expectations.

Fig. 4 displays the behavior of the various $e^+e^- \rightarrow \pi^+\pi^-$ data samples in the $(0.85 \div 1.2)$ GeV energy region. Here also the predicted curve accounts well for the data behavior. A closer inspection tells that the sparse NSK data are well described. The BaBar data are also well accounted for all along this energy interval except for the ϕ region. As shown by Fig. (1c) above, this can be cured and one can show that the difference is mostly due to the phase for the $\phi \rightarrow \pi^+\pi^-$ amplitude which departs significantly²⁰ from those provided by SND [48]. One could also note that both KLOE data samples look slightly below the τ +PDG expectations in this region.

One may conclude from Figs. 3 and 4 that our " τ +PDG" predictions are in good agreement with the data and that a fit using fully these data samples should provide marginal differences between all $\pi^+\pi^-$ data sets²¹.

However, the picture becomes quite different in the medium energy region $(0.70 \div 0.85)$ GeV as illustrated by Figure 5. In this region, our τ +PDG prediction follows almost perfectly expectations²¹ from both KLOE08 and KLOE10 data and the detailed lineshape at the $\omega - \rho$ interference region is strikingly reproduced. Paradoxically, the NSK data are slightly less favored – especially around 0.8 GeV – despite their influence on the PDG information used in order to account for IB effects in the $\omega - \rho$ interference region; however, taking into account experimental uncertainties, we already know that a global fit using NSK data is highly successful [13].

In contrast, the behavior of the BaBar data looks inconsistent with the τ +PDG prediction, especially on the low mass side of the interference region. Actually, the observed overestimate of the BaBar spectrum affects the whole region from threshold to the ω mass but is more important in the range $(0.74 \div 0.78)$ GeV. At higher energies one observes a reasonable agreement with expectations as well as with both KLOE data sets.

One should also note that the ω mass and (total) width induced by the data for the $\pi^0\gamma, \eta\gamma, \pi^+\pi^-\pi^0$ final states are in perfect agreement with all the examined data samples; this indicates that the energy calibration around the ω mass is good for all ISR data samples. Fig. (1c) has already shown that the BaBar energy calibration is also good in the ϕ region.

4.2 Predictions Using the $\rho^0 - \omega$ Interference Region From Data

As stated in Subsection 3.1, one can replace the PDG information for $\omega \rightarrow \pi^+\pi^-$ and $\rho^0 \rightarrow e^+e^-$ by any pion form factor spectrum limited to the region $(0.76 \div 0.82)$ GeV. In

²⁰ This issue is examined in detail in Subsection 5.1.4 below.

²¹ Precise information concerning fit qualities is ignored in this Section.

particular, this turns out to fit $F_\omega = \text{Br}(\omega \rightarrow e^+e^-) \times \text{Br}(\omega \rightarrow \pi^+\pi^-)$ and the Orsay phase as it comes out from each of the specified data sets.

Concerning the $\phi \rightarrow \pi^+\pi^-$ mode, one can also check the BaBar data [33, 34] versus the SND data [48]. This will be discussed below in the context of global fitting (see Subsection 5.1.4).

Using the NSK data or any of both KLOE samples instead of the PDG data does not lead to predicted spectra substantially different from their analogue already shown and commented upon in the previous Subsection. Some additional parameter constraints have been derived from global fits using only the $(0.76 \div 0.82)$ GeV region from the NSK and KLOE spectra for $e^+e^- \rightarrow \pi^+\pi^-$; the corresponding results are given in Table 1 and are in reasonable agreement with RPP expectations for the branching ratio product F_ω and the Orsay phase [46, 47] as well.

As far as BaBar is concerned, the situation looks different and the most relevant piece of information is provided in Figure 6. This proves that the largest difference between BaBar data and the other analogous data samples [27, 29, 31, 32] is the F_ω information inherent to the BaBar data. With a $(7 \div 8)\sigma$ difference with expectations, the BaBar value for F_ω is in clear conflict with the RPP value, while NSK and both KLOE values are in much better accord. This strong disagreement is substantiated by comparing Figures 5 and 6. More precise information can be read off Table 1.

Data Sample	Local Fit		
	$F_\omega 10^6$	Orsay Phase (degrees)	Prob. (%)
Input values [24, 46]	1.225 ± 0.071	104.7 ± 4.1	—
PDG Refitted value	1.157 ± 0.053	108.92 ± 2.36	89.4%
NSK [27, 29]	1.219 ± 0.043	106.71 ± 0.25	90.0%
KLOE08 [31]	1.076 ± 0.041	110.44 ± 1.24	87.8%
KLOE10 [32]	0.973 ± 0.045	113.62 ± 1.63	92.7%
BaBar [33]	1.780 ± 0.011	107.50 ± 0.19	54.4%

Table 1: Fit results for $F_\omega \doteq \text{Br}(\omega \rightarrow e^+e^-)\text{Br}(\omega \rightarrow \pi^+\pi^-)$ and for the Orsay phase (in degrees) using only the $(0.76 \div 0.82)$ GeV energy region of each $\pi^+\pi^-$ data sample. The fit is done following the (local) procedure sketched in Subsection 4.2.

4.3 Isospin Breaking Effects in the BHLS Model : Comments

It follows from the developments just above that the BHLS model fed with a limited number of accepted values for some IB pieces of information is indeed able to provide a quite satisfactory prediction for the $e^+e^- \rightarrow \pi^+\pi^-$ cross section once the τ spectra are considered.

This gives support to our breaking model, especially to the s -dependent vector meson mixing mechanism.

The prediction is found in accord with the scan (NSK) data samples and with both KLOE data sets²². Indeed, the predicted lineshape strikingly follows the central values from both KLOE data samples; for the scan data, the prediction based on PDG information is good but not as good as for the KLOE data. However, we have shown that changing the PDG requested IB information by less than 1σ – as following from a mere comparison of the first and second lines in Table 1 – leads to a perfect description of the NSK spectra over the whole available energy range. In contrast, the RPP branching fraction product F_ω has to be changed by about 7σ in order to yield a comparable description of the BaBar [33] data.

Basically, our approach is a τ based prediction of $\pi^+\pi^-$ spectra; it relies on the consistency of several different physics channels, the τ spectra and on a model of isospin symmetry breaking. It is thus interesting to examine the consequences of this τ based approach on the muon $g - 2$ estimated value. This is what is shown in Figure 7. The first line displays the results obtained using the $\rho \rightarrow e^+e^-$ partial width, the F_ω and F_ϕ values extracted from the RPP [24] and the two phases already quoted (pure “ τ +PDG” prediction). The four following lines are obtained by replacing the ρ and ω IB information by the $0.76 \div 0.82$ GeV region of the quoted data sets. The line named BNL displays the experimental result [39, 40] and the last line shows the τ based estimate from [8]. The behavior of the BaBar form factor on the mass interval $[2m_\pi, m_\omega]$ compared with expectation explains the difference we get for $g - 2$ compared with [34].

It is clear that all methods used to include IB effects within our τ based approach give consistent results, all distant from the BNL measurement at the 4σ level.

5 Global Fits Using the $e^+e^- \rightarrow \pi^+\pi^-$ Spectra

As in our previous analysis [13], we have performed global fits using simultaneously all e^+e^- annihilation data into the $\pi^0\gamma, \eta\gamma, \pi^+\pi^-\pi^0, K^+K^-, K^0\bar{K}^0$ final states, the dipion spectra collected in the decay of the τ lepton [21, 23, 22] and the decay information listed in Subsection 3.1. We also use the RPP ϕ decay properties in the (updated) way emphasized in Subsection 3.3.

For what concerns the $e^+e^- \rightarrow \pi^+\pi^-$ data included into the global fit procedure, we have performed fits using separately the NSK, KLOE08 and KLOE10 data samples. Global fits have also been performed for the BaBar dipion spectrum restricted to the range of validity of our BHLS model. Two options have been considered, using BaBar data up to 1 GeV supplemented by $\phi \rightarrow \pi^+\pi^-$ decay properties from the RPP or using BaBar data up to 1.05 GeV, thus including the BaBar ϕ region and avoiding the need to use RPP information about the ϕ . In all cases, the errors (and the χ^2) were constructed following the information published/recommended by the experimental groups who collected these data.

We have also performed global fits using combinations of these individual $\pi^+\pi^-$ data samples. In this case, the contributions of the NSK and KLOE10 data to the total χ^2 were left unweighted as their own χ^2/n contribution is always of the order 1 in fits using each of them

²²Some issue with the uncertainties of the KLOE08 data sample will be discussed below.

in isolation²³. In contrast, in such combinations involving the KLOE08 and/or BaBar data, the contribution of each of these to the total χ^2 was weighted by the ratio $f_M = n_M/\chi_M^2$ (M= KLOE08, BaBar) where χ_M^2 is the χ^2 of the M data set obtained in the best fit using only M as $e^+e^- \rightarrow \pi^+\pi^-$ data set; n_M is the corresponding number of data points. In fits involving the spacelike data [35, 36], the corresponding weight was also used²⁴.

For definiteness, when relevant, we have used $f_{NSK} = f_{KLOE10} = 1$, $f_{KLOE08} = 60/90 \simeq 0.67$, $f_{BaBar} = 270/346 \simeq 0.78$ and $f_{space} = 59/85 \simeq 0.69$. These weights have been varied and it has been found that the sensitivity of the physics results to their precise value is marginal; the main virtue of these weights is to provide probabilities not too much ridiculous.

We have preferred using this method, which turns out to consider each data set as a global object, rather than defining local (s -dependent) averages as done by others [6]. This method looks better adapted to the global fit method which provides a quality check reflecting the behavior of each $e^+e^- \rightarrow \pi^+\pi^-$ data set within the global context of a large number of physics channels. Indeed, doing local averages would prevent to detect discrepancies originating from some given data set only.

For completeness, it is worth noting that the χ^2 contributions of the – more than 40 – data sets associated with all the other channels were always left unweighted.

A feature common to all fits using the $e^+e^- \rightarrow \pi^+\pi^-$ data sets in isolation or combined is that the individual χ^2 contributions associated with the other channels ($\pi^0\gamma$, $\eta\gamma$, $\pi^+\pi^-\pi^0$, K^+K^- , $K^0\bar{K}^0$, ...) were only marginally affected by the specific choice of $e^+e^- \rightarrow \pi^+\pi^-$ data submitted to fit. Their typical values are almost identical to what can be found in the last data column of Table 3 in [13]; more precisely, the χ^2 value provided by each of these channels never varies by more than a few percents. Let us remind that the number of data points submitted to fit – beside the $e^+e^- \rightarrow \pi^+\pi^-$ data – is $\simeq 600$ when working within²⁵ the configuration B defined in [13] ($\simeq 675$ within configuration A).

5.1 Salient Features of the Various $e^+e^- \rightarrow \pi^+\pi^-$ Spectra

We have performed several tens of fits of the various $e^+e^- \rightarrow \pi^+\pi^-$ spectra in standalone mode and/or combined. It does not look useful to report on each fit in detail. Instead of overwhelming the reader with unnecessary information and plots, we have preferred focusing on the salient features of their behavior within the global fit context. Beside the fit properties of the full spectra (up to 1 GeV, generally), this covers the muon anomalous magnetic moment value and the behavior at the ω mass, more precisely the value for $F_\omega = \text{Br}(\omega \rightarrow e^+e^-) \times \text{Br}(\omega \rightarrow \pi^+\pi^-)$. The first of these topics will be addressed in a separate Section below. Concerning the second topic, one reminds that the value for F_ω expected from the RPP is $(1.225 \pm 0.071) \cdot 10^{-6}$, while the τ +PDG outcome is rather $(1.157 \pm 0.053) \cdot 10^{-6}$.

On the other hand, we do not enter into much detail concerning the effects of the spacelike data, always used weighted in this paper; we limit ourselves to mentioning that they never

²³ We use the wording "in isolation", "isolatedly", or "standalone" to qualify fits performed using a specific $e^+e^- \rightarrow \pi^+\pi^-$ data sample. It should be reminded that this $\pi^+\pi^-$ data set is *always* fitted together with all the other data listed in Subsection 3.1, unless otherwise stated.

²⁴ In the fits referred to in [49], the spacelike data contributions to the total χ^2 were left unweighted.

²⁵ The difference between configuration B and configuration A is that the former excludes the use of the 3-pion data collected around the ϕ mass.

modify the fit qualities in a significant way.

5.1.1 Standalone Fits of the $e^+e^- \rightarrow \pi^+\pi^-$ Spectra

When using only²³ the (unweighted) NSK data, the fit returns²⁶ $\chi_{NSK}^2/N_{\pi^+\pi^-} = 128.30/127$ and a global fit probability of 96.3%. We do not show the fit residuals for the scan data which are quite similar to Figure 5 in [18].

Similarly, the KLOE10 data set [32] returns $\chi_{KLOE10}^2/N_{\pi^+\pi^-} = 73.68/75$ and a global fit probability of 87.7%. The fit residual distribution is shown in the top panel of Figure 8; the bottom panel in this Figure shows the fractional deviations from the fitting function. Both distributions can be considered as reasonably flat. In order to draw the plots, we have used as uncertainties the square root of the diagonal elements of the (full) error covariance matrix. Therefore, the value for χ_{KLOE10}^2 and the flatness of the residuals shown in Figure 8 illustrate that the full error covariance matrix is correctly understood.

Therefore, within the global fit context, each of the NSK and KLOE10 data samples exhibits the same outstanding behavior²⁷. On the other hand, the fit parameters and error covariance matrix allows to derive, using obvious notations, $F_{\omega}^{NSK} = (1.205 \pm 0.042) 10^{-6}$ close to the PDG value reported at top of Table 1. One also gets $F_{\omega}^{KLOE10} = (1.074 \pm 0.051) 10^{-6}$, a $\simeq 2.5\sigma$ difference with the central value for F_{ω}^{NSK} .

Under the same conditions, the (unweighted) KLOE08 data set returns $\chi_{KLOE08}^2/N_{\pi^+\pi^-} = 96.55/60$ and a global fit probability of 56%, which is rather low. It is worth noting the remarkable flatness of the residual distributions displayed by Figure 9 which does not prevent to yield a relatively large value for χ_{KLOE08}^2 . The large χ_{KLOE08}^2 and the flatness of the residual distribution shown in Figure 9, considered together, might indicate an issue with the non-diagonal part of the full error covariance matrix. Anyway, one can conclude that the poor KLOE08 fit probability reflects an issue with the KLOE08 error estimate rather than a distorted lineshape.

Figure 9 should be compared with the similar distribution derived formerly using a primitive version of the BHLS model (see Figure 3 in [19]). The clear improvement substantiates the gain provided by the BHLS model in its present form. On the other hand, one should also note that the value for $F_{\omega}^{KLOE08} = (1.117 \pm 0.042) 10^{-6}$ is consistent with F_{ω}^{KLOE10} .

The fit of the (unweighted) BaBar data leads to $\chi_{BaBar}^2/N_{\pi^+\pi^-} = 343.08/270 = 1.27$ when limited to 1 GeV (17% probability) and to $\chi_{BaBar}^2/N_{\pi^+\pi^-} = 340.77/275 = 1.24$ when going up to 1.05 GeV (corresponding to a 22% probability). For reasons already noted, these probabilities are relatively low, reflecting an issue with the rest of the physics involved in the global fit, especially the τ data. Qualitatively, this result could have been expected from the τ +PDG predictions already discussed. The residual distributions are given in Figure 10 and look reasonable. The residual distribution corresponding to fitting up to 1.05 GeV clearly shows a modified behavior in the ω region. This has some consequence on the BaBar estimate of the muon anomalous moment, as will be emphasized in Subsection 6.1 below. Finally, it is interesting to note that the fit outcome provides $F_{\omega}^{BaBar} = (1.628 \pm 0.012) 10^{-6}$ (fit up to

²⁶ The agreement of this result with the corresponding one given in Table 3 of [13] clearly proves that the modification of the $\phi \rightarrow \pi^+\pi^-$ information is marginal for the fits not containing the ϕ region. The latter is covered by the BaBar data set only.

²⁷ As emphasized in our previous works [19, 20, 13], the global probabilities are enhanced thanks to the highly favorable fit properties of the $e^+e^- \rightarrow (\pi^0/\eta)\gamma$ data; indeed, χ^2/N for these are respectively $\simeq 0.76$ and 0.66 .

1 GeV) or $F_{\omega}^{BaBar} = (1.575 \pm 0.010) 10^{-6}$ (fit up to 1.05 GeV), both being far from F_{ω}^{NSK} , $F_{\omega}^{KLOE08/10}$ and from expectations [24].

5.1.2 Fits Combining the $e^+e^- \rightarrow \pi^+\pi^-$ Spectra

In view of the standalone fits just reported, we have done fits of different combinations of the scan (NSK) and ISR data samples. In this case, the contributions of the KLOE08 and BaBar samples to the (minimized) χ^2 function are *always* weighted as already stated.

- Combining the KLOE08 and KLOE10 data : This returns a consistent picture where χ_{KLOE10}^2 and χ_{KLOE08}^2 are almost unchanged compared to their standalone values and the fit probability reaches 81.6 %. This, indeed, confirms that they share the same physics content. This is confirmed by the fit result $F_{\omega}^{KLOE08/10} = (1.121 \pm 0.038) 10^{-6}$, consistent with both of F_{ω}^{KLOE08} and F_{ω}^{KLOE10} .
- Combining all the ISR data sets (KLOE08, KLOE10 and BaBar) : This returns $\chi_{ISR}^2/N_{\pi^+\pi^-} = 1.34$ when including the weights for KLOE08 and BaBar and $\chi_{ISR}^2/N_{\pi^+\pi^-} = 1.64$ when the weights are not included. The weighting used does not prevent the probability to remain poor²⁷ (1.8%) reflecting the level of inconsistency of the BaBar and KLOE(08/10) data samples already noted. In this case, one gets $F_{\omega}^{ISR} = (1.608 \pm 0.010) 10^{-6}$, exhibiting a large distortion towards the BaBar lineshape, despite the weighting.
- Combining all $e^+e^- \rightarrow \pi^+\pi^-$ spectra : Taking the weights into account – which is more favorable – one gets $\chi_{Global}^2/N_{\pi^+\pi^-} = 1.35$ and a fit probability²⁷ of 1.3%. Once again, the lineshape of the fit function is highly influenced by the BaBar sample in the $\rho - \omega$ interference region as shown by $F_{\omega}^{Global} = (1.582 \pm 0.089) 10^{-6}$.
- Combining the NSK and KLOE10 data : In this case, there is no weight and one gets $\chi_{NSK}^2/N_{\pi^+\pi^-} = 131.37/127$ and $\chi_{KLOE10}^2/N_{\pi^+\pi^-} = 72.90/75$ close to the standalone²³ fit results, *i.e.* $\chi_{KLOE10+NSK}^2/N_{\pi^+\pi^-} = 1.01$, and the remarkable global fit probability of 96.9 %, showing that the NSK and KLOE10 data samples are quite consistent with each other and with the rest of the BHLS physics as well. In this case, one also yields

$$F_{\omega}^{NSK+KLOE10} = (1.166 \pm 0.036) 10^{-6},$$

which should supersede the present world average value [24] because of the full consistency it exhibits with the largest set of data ever fitted simultaneously and with a splendid probability.

5.1.3 Fits of the $e^+e^- \rightarrow \pi^+\pi^-$ Spectra : Concluding Remarks

The results reported just above have allowed us to show that the NSK data are in fair agreement with the physics represented by the $\pi^0\gamma$, $\eta\gamma$, $\pi^+\pi^-\pi^0$, K^+K^- , $K^0\bar{K}^0$ annihilation channels, the dipion spectra collected in the decay of the τ lepton and some more decay information listed in Subsection 3.1. This is not a really new result as this conclusion was already reached in our [13]. The single difference with [13] is the new dealing with the $\phi \rightarrow \pi^+\pi^-$ information (see Subsection 3.3) imposed by the BaBar data.

The new information is that the KLOE10 data sample behaves likewise and, more importantly, that the NSK and KLOE10 data sets are consistent with each other as well as with the rest of the physics considered within the BHLS model and the global fit context.

We have performed global fits which have shown that the data from KLOE08 and BaBar have some difficulty to accommodate the global fit context. For what concerns KLOE08, the problem appears to be related with (underestimated?) systematic errors or, possibly, with their correlations. In the case of BaBar data, the problem looks more serious, as it deals with the form factor lineshape itself in the $\rho - \omega$ interference region; this issue manifests itself in the value for F_ω , much larger than expected.

For this purpose, it is interesting to see the behavior of the most relevant fits of the pion form factor in the $\rho - \omega$ resonance region. These are displayed in Figure 11. The best fit obtained using only the NSK data is shown in the top left panel and is clearly quite satisfactory. The top right panel exhibits the case when the NSK data are complemented with the KLOE10 sample; this fit is also quite successful.

Bottom left panel in Figure 11 shows the behavior of the best fit function when only considering the ISR data (BaBar, KLOE08, KLOE10) and bottom right panel when taking into account all existing scan and ISR data. Both are clearly less satisfactory reflecting mostly the tension between BaBar and the KLOE data sets.

The question is now whether the KLOE08 and BaBar data samples can nevertheless help to improve some physics information of important concern as the muon $g - 2$. This will be discussed in the forthcoming Section. Anyway, the KLOE10 data sample allows to confirm the results already derived using the NSK data and, even, helps in getting improved results.

5.1.4 The ϕ Region in the $e^+e^- \rightarrow \pi^+\pi^-$ Spectrum

Up to now, the ϕ pieces of information used in our fits/predictions are the RPP value for the product $F_\phi = \text{Br}(\phi \rightarrow e^+e^-)\text{Br}(\phi \rightarrow \pi^+\pi^-) = (2.2 \pm 0.4) 10^{-8}$ and the "Orsay" phase for the $\phi \rightarrow \pi^+\pi^-$ amplitude provided by SND [48], namely -34.0 ± 4.0 degrees. In order to avoid over interpreting the SND phase as an Orsay phase (*i.e.* identified with the phase of the product $F_{\omega\phi}^e(s) g_{\phi\pi\pi}(s)$ in Eq. (11) at $s = m_\phi^2$), we have found worth revisiting this assumption. Using the NSK and KLOE10 data sets as reference $\pi^+\pi^-$ data sample, we have performed several global fits within the BHLS framework.

For definiteness, and for an easy comparison, the first line in Table 2 displays the values extracted from [24, 48] and used in all fits referred to up to now. The second line in this Table displays the corresponding values reconstructed using the final parameter values from the appropriate global fit. The goodness of fit (94.5% probability) is reflected by the χ^2 values shown in the last two data columns. The reconstructed value for F_ϕ is in very good accord with the (input) RPP value, while the phase is shifted toward slightly more negative values than the SND datum.

The fit results summarized in the third line are obtained by withdrawing the SND phase [48] from the minimization procedure. The fit quality is almost unchanged (95.3% probability) and the expected F_ϕ is still well reproduced; on the other hand, the ϕ phase moves by about 3σ but remains significantly negative.

In both cases, the pion form factor lineshape exhibits the behavior shown in Figure (1b), e.g. a tiny peak at the ϕ mass, resembling what is shown in Figure 4 of [48].

The next step has been to remove the reference values for F_ϕ and for the ϕ phase and supplement the NSK and KLOE10 data with the ϕ region spectrum from BaBar data ($\sqrt{s} \in [1.00, 1.05]$ GeV). The important results are shown in the fourth line of Table 2. The fit probability remains good (91.3%), but the χ^2 of the NSK+KLOE10 data is degraded by $\simeq 10$ units, which may indicate some tension between these data sets and the coherent background beneath the ϕ peak. The fit value for F_ϕ increases by 50% but remains perfectly consistent with expectations [24]. In contrast, the Orsay phase changes dramatically (from $-[30 \div 50]^\circ \rightarrow 150^\circ$). The lineshape exhibited by the BaBar pion form factor is almost identical to those shown in Figure (1c).

ϕ Information Used	$F_\phi 10^8$	Orsay Phase	$[\chi^2_{\pi^+\pi^-}/N_{points}]_{<1.0 \text{ GeV}}$	$[\chi^2_{\pi^+\pi^-}/N_{points}]_\phi$
Input [24, 48]	2.2 ± 0.4	-34.0 ± 4.0	-	-
Imposing Orsay phase [48]	2.34 ± 0.42	-41.45 ± 1.89	204.3/202	2.25/2
Releasing Orsay phase	2.23 ± 0.41	-48.23 ± 1.88	202.9/202	0.04/1
BaBar ϕ Region Spectrum [33]	3.31 ± 0.99	156.92 ± 2.76	215.0/202	5.2/5
BaBar data [33] fit	3.04 ± 0.60	153.41 ± 0.98	(338.1/270)	(2.69/5)
Imposing BaBar ϕ parameters	3.05 ± 0.50	153.37 ± 0.85	208.0/202	0.05/2

Table 2: Fit results for $F_\phi = \text{Br}(\phi \rightarrow e^+e^-)\text{Br}(\phi \rightarrow \pi^+\pi^-)$ and for the "Orsay" phase (in degrees) for the ϕ amplitude. See Subsection 5.1.4 for comments.

As stated above¹⁵, the $[1.00, 1.05]$ GeV region of the BaBar spectrum carries information on the ϕ signal but also on the underlying (ρ coherent) background. In order to substantiate its effect, we have finally performed a fit using as input the F_ϕ and ϕ phase values extracted from fitting the BaBar data up to 1.05 GeV (see Subsection 5.1.1); the corresponding values are given in the fifth data line of Table 2 and, when imposed to the fit procedure, these numbers lead to the results shown in the last line. The fit probability improves to 94%.

As a summary, Table 2 shows that some ambiguity occurs about the pion form factor behavior in the ϕ region. It becomes interesting to have new data covering this region, in order to decide which among Figures (1b) and (1c) reflects the right behavior. It is also interesting to examine the consequences of this ambiguity on $g - 2$ estimates.

Without going into details (addressed in the next Section), we can give the values for $\Delta a_\mu = a_\mu^{exp} - a_\mu^{th}$ corresponding to the various cases shown in Table 2. In units of 10^{-10} , the values for Δa_μ are respectively 39.91 ± 5.21 (line # 2), 39.35 ± 5.23 (line # 3), 37.18 ± 5.16 (line # 4) and 39.32 ± 5.20 (line # 6). The most likely effect this implies on Δa_μ is a possible *shift* by 0.59×10^{-10} (lines # 2, 3, 6). A maximum possible shift is 2.73×10^{-10} (lines # 2 and 4). Instead, the uncertainty is practically unchanged. Taking into account the uncertainty on a_μ^{exp} [39, 40], the significance implied by this shift is quite marginal (from 4.88σ to 4.57σ). Nevertheless, this shift plays as a systematic effect to be accounted in the final value which will be proposed for a_μ^{th} .

6 Hadronic Contribution to the Muon $g - 2$ Estimates

In order to estimate the hadronic contribution to the muon anomalous magnetic moment a_μ , the method followed in the present work is identical to the one used in [13]. In this Section, we examine the global fit solutions provided by the data samples listed in Subsection 3.1; the various cases correspond to varying the $e^+e^- \rightarrow \pi^+\pi^-$ data sample combination submitted to the global fit procedure.

In our previous analysis [13], we encountered some tension in the e^+e^- annihilation data in the ϕ region between the $e^+e^- \rightarrow \pi^+\pi^-\pi^0$ channel and the $e^+e^- \rightarrow K^+K^-, K^0\overline{K}^0$ channels. Including all data in the global fit defined what we called "configuration A". Alternatively, we excluded the 3-pion data in the vicinity of the ϕ mass from the fit. In this case, the corresponding collection of data included in the fit was called "configuration B", which yields a better fit probability. As [13], the present analysis privileges configuration B as a basis. As the "observed" tension could not be abnormal, we also consider fits based on configuration A for completeness.

6.1 $a_\mu(\pi\pi)$ Contribution from the Reference $m_{\pi\pi}$ Region

In order to emphasize what is going on, it is worth examining the contribution to $a_\mu(\pi\pi)$ provided by the invariant mass interval $\mathcal{A} \equiv [0.630, 0.958]$ GeV. As for this reference region, all experimental groups have published the numerical integration leading to their estimate of $a_\mu(\pi\pi, \mathcal{A})$ (using Eq. (1) with the experimental spectra), one can compare our fit outcome with these. When combining data sets within the fit procedure, we compare to the usual weighted average of the $a_\mu(\pi\pi, \mathcal{A})$ values provided by each experimental group.

The results for $a_\mu(\pi\pi, \mathcal{A})$ are collected in Fig. 12 and will be discussed from top to bottom. The first point has no experimental partner, as it comes out from the τ +PDG fit described in Section 4. The dashed-dotted line is drawn through the central value of this prediction, the dotted lines show the corresponding $\pm 1\sigma$ band.

It should then be noted that most experimental estimates happen to be inside the 1σ band of the τ +PDG prediction. KLOE10 is at the border, while BaBar is rather larger by about 2σ . One should also note that KLOE08 as well as the combination CMD2+SND+KLOE10 (our preferred combination because of its global fit properties) provide central values which coincide almost exactly with the τ +PDG expectation. This looks to us a noticeable property taking into account the long-standing discussion about the $\tau - e^+e^-$ issue. Our results tend to prove that this issue vanishes once the breaking mechanism is appropriate.

The next point shows the global fit estimate (square symbol) while using solely the NSK data (especially those from [27, 28, 29], but also those from [25, 26]). The present fit value is found smaller than those published in [13] by about 1×10^{-10} . This shows that the effect of our updating the ϕ data decay information extends over the whole spectrum. The uncertainty is unchanged and amounts to a 40% gain compared with the experimental estimate. This gain is a pure effect of the global fit procedure where the channels others than $\pi^+\pi^-$ allow to improve *also* the $\pi^+\pi^-$ contribution importantly because of the underlying VMD physics correlations.

The following point is derived using solely the KLOE08 data sample. As with fitting solely the NSK data, the fit outcome also differs by 1×10^{-10} from the experimental central value. The fit result associated with the KLOE10 data sample is also found in good agreement with

the experimental expectation and one should note that both differ by 1.5×10^{-10} in the opposite direction. In contrast, the fit result for the mixed KLOE10+(weighted) KLOE08 data sample is found to agree very well with expectation (a 0.6×10^{-10} difference only).

The data point associated with the CMD2+SND+KLOE10 combined data sample is found in much better accord with the average of the experimental data; in this case, the error is also improved by about a factor 2 compared with the experimental value, but, interestingly, first, the central reconstructed value does not exhibit any significant systematic shift ($\simeq 0.1 \times 10^{-10}$) compared to the experimental expectation, second, the central reconstructed value is in perfect accord with the τ +PDG prediction, as already noted.

The next pair of points shows the case for the BaBar data. While using the whole spectrum up to 1 GeV, the fitting function provides an estimate for $a_\mu(\pi\pi, \mathcal{A})$ in good agreement with the expected experimentally integrated value. However, extending the fitting region up to 1.05 GeV, increases the difference between the fit outcome and the experimental expectation from 1.5×10^{-10} to 4.4×10^{-10} , which illustrates some issue when fitting also the BaBar ϕ region.

The last two points (ISR and scan + ISR data, resp.) correspond to fitting the whole spectra up to 1 GeV while weighting the KLOE08 and BaBar contributions to the χ^2 . The results look in good correspondence with the weighted averages of the direct integration results, and one remains within the 1σ band of the τ +PDG expectation.

The contribution to $a_\mu(\pi\pi)$ from the invariant mass interval $\mathcal{A} \equiv [0.630, 0.958]$ GeV and the global fit properties (see Section 5) allow to draw a few important conclusions :

- **(I)** There is no mismatch between the τ +PDG expectations and the estimates derived from the fitting functions or those derived from the numerical integration of the measured $e^+e^- \rightarrow \pi^+\pi^-$ cross sections. To be more precise, when some departure is observed, it is always closely associated with poor global fit qualities of the corresponding data sample.
- **(II)** One can take as reference $e^+e^- \rightarrow \pi^+\pi^-$ data the NSK (CMD-2 & SND) and KLOE10 data samples. Separately and together, they are found in perfect accord with all annihilation data considered ($\pi^0\gamma$, $\eta\gamma$, $\pi^+\pi^-\pi^0$, K^+K^- , $K^0\bar{K}^0$ final states) as well as with the published dipion spectra in the decay of the τ lepton and the few additional decay information introduced within the global fit BHLS framework. The uncertainty is improved by a factor of about 2.
- **(III)** Comparing the central value for $a_\mu(\pi\pi, \mathcal{A})$ derived from the fitting function – using the NSK and KLOE10 data samples within the global framework – with its direct estimate indicates that the estimate derived from the fit is almost unbiased ($\simeq 0.1 \times 10^{-10}$). In contrast, the fitting functions derived from the fits to each of the NSK and KLOE10 data separately may exhibit a small bias (a shift of $\simeq 1 \times 10^{-10}$).
- **(IV)** One may remark that the global fit using all existing $e^+e^- \rightarrow \pi^+\pi^-$ scan & ISR data also provides reasonable values for $a_\mu(\pi\pi, \mathcal{A})$ without a significant bias and with a much improved uncertainty. This reduced uncertainty may look too optimistic, taking into account the global fits properties of the corresponding sample combinations.

6.2 The Full Muon Anomalous Magnetic Moment a_μ

Here we are interested in the theoretical prediction of the muon anomalous magnetic moment and its comparison with the experimental result [39, 40]. Our BHLS based global fit results provide the dominant contribution to the hadronic vacuum polarization contribution.

Several global fits have been performed using different groups of $e^+e^- \rightarrow \pi^+\pi^-$ data samples. The resulting fitting functions and the parameter error covariance matrices have allowed to derive the leading order hadronic contribution (LO-HVP) to a_μ up to 1.05 GeV in various cases. The full HVP is obtained by combining our present results with the other hadronic contributions listed in Table 9 of our previous work [13]. The various evaluations of the muon $g - 2$ are calculated by summing up a_μ^{LO-HVP} with the Higher order HVP, the QED and the electroweak (EW) contributions and the so-called light-by-light (LBL) contribution; for this purpose, the values given in Table 10 of [13] have been updated (see Table 3 below).

In Figure 13, we display results for the deviation $\Delta a_\mu = a_\mu^{\text{exp}} - a_\mu^{\text{th}}$ between experiment and theoretical predictions in units of 10^{-10} , for various fit results which only differ by the indicated $e^+e^- \rightarrow \pi^+\pi^-$ data sample considered within the fit procedure.

Specifically, the fit results included in Fig. 13 are all based on the “configuration B” data set introduced in [13]. Furthermore, always included in the fits are all channels listed in Subsection 3.1, especially the τ data.

At top of the Figure, we provide the τ +PDG entry (*i.e.*, without using any $e^+e^- \rightarrow \pi^+\pi^-$ data set in the fit procedure). The twin points drawn correspond to $\Delta a_\mu = a_\mu^{\text{exp}} - a_\mu^{\text{th}}$ in units of 10^{-10} ; the lower point is obtained using the spacelike data [35, 36], the upper one by excluding them from the fit. The number following the point is the estimate for Δa_μ from fits excluding the spacelike data. The significance of this difference is written $[x/y \sigma]$, $x\sigma$ being the significance obtained when excluding the spacelike data, $y\sigma$ when they are included into the fit procedure. The last column in this Figure provides the χ^2/n_{points} for the $e^+e^- \rightarrow \pi^+\pi^-$ data; this number is given only for (combination of) samples used without any weight.

The first remark which can be drawn is that including the spacelike data does not change noticeably the value for Δa_μ nor its statistical significance. The second important point is that all the features noted while discussing $a_\mu(\pi\pi, [0.630, 0.958] \text{ GeV})$ in the previous Subsection survive when dealing with the whole provided spectra (see (I)–(IV) just above).

It was noted in [13] that the use of the ISR data should not dramatically improve the uncertainty of the theoretical estimate : going from scan data only (the NSK entry) to scan+ISR data (the “Global Fit” entry) improves the uncertainty by only 0.3×10^{-10} ; this is the major gain of working in a global fit context [13]. In contrast, the central value exhibits slightly more sensitivity, as can be seen by comparing the various entries.

Anyway, the present analysis allows to conclude that the discrepancy between the measurement for a_μ [39, 40] and the Standard Model prediction is certainly in the range of 4.5σ or slightly higher. Taking into account the already reported fit qualities, the most favored value for a_μ^{LO-HVP} is :

$$a_\mu^{LO-HVP} = (681.23 \pm 4.51) 10^{-10}. \quad (13)$$

This value is derived by introducing the e^+e^- NSK and KLOE10 data samples within our global fit procedure.

Finally, we have redone several of our fits within the configuration A. These confirm the results derived within the configuration B which are the body of the present paper. One also

confirms the ‘tension’ reported in [13] between the 3–pion spectra in the ϕ region and the data collected for both $e^+e^- \rightarrow K\bar{K}$ cross sections. Whether this is an experimental issue, or if this indicates that our breaking model should be extended²⁸ is an open issue. Nevertheless, some physics results derived within the configuration A will be presented just below.

6.3 Comparison with Other Estimates of a_μ

Fig. 14 reports on some recent estimates of the muon anomalous magnetic moment a_μ together with the BNL average value [39, 40]. In this Figure, our (favored) results – derived using only the CMD–2, SND and KLOE10 data samples – are given under the entry tags BHLS::A (for configuration A) and BHLS::B (for configuration B). Some evaluations proposed by other authors are also shown; they are extracted from [6] (DHMZ10), [7] (JS11), [8] (DHea09) and [9] (HLMNT11).

$10^{10}a_\mu$	Values (incl. τ)		Values (excl. τ)	
	scan only	scan \oplus ISR	scan \oplus ISR	scan only
LO hadronic	685.66 ± 4.54	688.60 ± 4.24	687.53 ± 4.34	684.25 ± 5.15
HO hadronic	-9.97 ± 0.09			
LBL	10.5 ± 2.6			
QED	$11\,658\,471.8851 \pm 0.0036$			
EW	$15.40 \pm 0.10_{\text{had}} \pm 0.03_{\text{Higgs,top,3-loop}}$			
Total Theor.	$11\,659\,173.48 \pm 5.23$	$11\,659\,176.42 \pm 4.89$	$11\,659\,175.35 \pm 5.06$	$11\,659\,171.89 \pm 5.77$
Exper. Aver.	$11\,659\,208.9 \pm 6.3$			
Δa_μ	35.43 ± 8.14	32.48 ± 8.03	33.56 ± 8.08	36.89 ± 8.54
Significance ($n\sigma$)	4.33σ	4.05σ	4.16σ	4.32σ

Table 3: The various contributions to $10^{10}a_\mu$. $\Delta a_\mu = a_\mu^{\text{exp}} - a_\mu^{\text{th}}$ is given in units of 10^{-10} . These results have been derived using *all* existing annihilation data samples (configuration A). The naming “scan” and “ISR” in the subtitles refers only to the $\pi^+\pi^-$ channel. For the measured value a_μ^{exp} , we have adopted the value reported in the RPP which uses the updated value for $\lambda = \mu_\mu/\mu_p$ recommended by the CODATA group [50].

The analyses reported in [6], [9] and [7] provide $g-2$ evaluations based on *all* existing data samples. In particular, all $\pi^+\pi^-$ data samples are used (ISR and scan) and all other existing annihilation data samples, especially the 3–pion data samples. These evaluations of $g-2$

²⁸One might have to revisit the possibility that nonet symmetry should also be broken in the vector meson sector as it is already done in the pseudoscalar sector.

may also include or not the τ data. Therefore, it is also instructive to give the results derived from BHLS under the same conditions, *i.e.* working in the so-called configuration A [13] and using *all* available ISR data samples beside the scan (NSK) data, whatever are the global fit probabilities. The corresponding results are reported at the "Full BHLS" entries in Fig. 14. More precise information is also provided in Table 3. However, one should note that, while the fit probabilities are good when using only the scan (NSK) data (90.6 % or 72.7 % respectively), they are below the 10^{-4} level²⁷ when all the ISR data samples are included. This reflects the statistical inconsistency between both KLOE data samples on the one hand and the BaBar data sample on the other hand.

We have explored this issue in cases including the τ data samples. Without going into much details, it looks worth to comment about fit qualities. The just reported probabilities bounded by 10^{-4} are worrying, taking into account that the problematic data samples have been weighted. For this purpose, we have first performed a fit discarding the BaBar data sample, to check the level of statistical inconsistency of NSK, KLOE10 and (weighted) KLOE08; the obtained fit probability is 61.6 % and the numerical results are almost identical to those already derived using only NSK and KLOE10. In particular, the scan data yield $\chi^2(NSK)/n = 136/127 = 1.07$ and $F_\omega = (1.11 \pm 0.03) 10^{-6}$, *i.e.* a limited distortion of the scan data description. The same exercise performed using NSK and (weighted) BaBar yield 12.4% probability but $\chi^2(NSK)/n = 171/127 = 1.35$ and $F_\omega = (1.52 \pm 0.04) 10^{-6}$; *i.e.* a severely degraded description of the scan data.

It should be noted that, when using all $\pi\pi$ data samples, the value returned by the BHLS model is close to JS11 [7]. An interesting point here is that [7] uses a mixing procedure ($\gamma - \rho - \omega$) parent to ours ($\rho - \omega - \phi$), while the IB effects are introduced differently in order to get the DHMZ10 result [6]. Comparing the Full BHLS values derived when using or not the τ spectra indicates that BHLS is much less sensitive to the use of the τ spectra than the method from [6] (compare the DHMZ10 entries). Finally, comparing DHea09 [8] and BHLS when no ISR data are considered, one observes a good consistency; this seems to indicate that the problem lays in the amount of isospin breaking compared with τ .

Comparing now all the BHLS results (BHLS::A, BHLS::B and Full BHLS) indicates a remarkable stability for $\Delta a_\mu = a_\mu^{exp} - a_\mu^{th}$ under various fit conditions. One should also note that the τ +PDG prediction is always in quite nice agreement with using any kind of configuration for $\pi\pi$ data samples (BHLS::A, BHLS::B and Full BHLS), including those discarding the τ spectra and the ISR data (see also Table 3).

Nevertheless, one should stress that, because of the poor fit quality yielded when using the KLOE08 and BaBar data samples beside the NSK and KLOE10 ones, we do not consider the results shown in Table 3 and in Fig. 14 under the entry tag "Full BHLS" as reliable. As a general statement, we prefer relying on estimates using only the NSK and KLOE10 data samples for which the probabilities are good ($\simeq 90\% \div 98\%$ for BHLS::B, $\simeq 56\% \div 73\%$ for BHLS::A). Numerically, the BHLS::B and BHLS::A estimates happen to be always close to each other. Nevertheless, we prefer favoring the BHLS::B result over BHLS::A for reasons already explained.

The statistical significance for $\Delta a_\mu = a_\mu^{exp} - a_\mu^{th}$ is displayed on the right-hand side of the Figure for each of the reported analyses. The updating of the $\phi \rightarrow \pi\pi$ treatment within our minimization code turns out to increase the significance for Δa_μ by about 0.5σ without any significant change in the fit qualities. The present study, however, has shown that this update is

highly favored by the ϕ information carried by the BaBar spectrum.

On the other hand, one should note that using *all* ISR data samples only leads to a $\simeq 4\%$ improvement for the uncertainty on a_μ^{th} compared with discarding all of them. This is actually, as reminded in the Introduction, a specific consequence of the global fit procedure.

Before closing this Section, it is worth remarking that the central values for a_μ^{LO-HVP} derived using scan data only or scan \oplus ISR are very close to each other. This is due to a numerical conspiracy of the BaBar and KLOE data samples : The former data tend to increase a_μ^{LO-HVP} and the latter to decrease it, by a quite comparable amount. Taking into account the above reported fit probabilities, the increase of a_μ^{LO-HVP} is not justified on statistical grounds; in contrast the decrease of a_μ^{LO-HVP} produced by KLOE10 (and also KLOE08) is supported by quite good probabilities of simultaneous fits of scan and KLOE data.

6.4 A Few properties of the Favored (NSK+KLOE10) Estimate For a_μ

It follows from the present study that a consistent data sample can be defined which allows to yield a reliable estimation of a_μ^{th} . This sample contains all the collected data samples covering the $\pi^0\gamma$, $\eta\gamma$, K^+K^- and $K_L K_S$ annihilation channels and the dipion τ spectra up to 1 GeV. It also contains the $\pi^0\pi^+\pi^-$ annihilation channel. For this last process, we prefer working within the so-called configuration B by excluding the data sets collected around the ϕ mass. However, as clear from Figure 14, taking them into account (configuration A) does not lead to substantial differences. Concerning the fundamental $\pi^+\pi^-$ annihilation channel, the statistical properties exhibited by the fits lead us to rely on using only the scan (NSK) and the KLOE10 data samples.

This leads us to conclude that the most favored value for $\Delta a_\mu = a_\mu^{exp} - a_\mu^{th}$ is 39.91 ± 5.21 (in units of 10^{-10}). Subsection 6.1 tends to indicate that this value should be almost unbiased.

However, the ambiguity about the choice of the Orsay phase discussed in Subsection 5.1.4 may also indicate a possible systematic shift, likely of 0.59×10^{-10} , but certainly limited to 2.73×10^{-10} . This upper bound supposes that the BaBar spectrum behavior in the ϕ region should be trusted²⁹. Only a devoted measurement of the pion form factor in the ϕ region may allow to conclude about this possible systematic shift.

Looking at the differences between BHLS::A and BHLS::B, one also observes that the most significant difference between both solutions is concentrated – as could be expected – in the contribution of the 3-pion data around the ϕ peak. This may lessen Δa_μ by 1.26×10^{-10} .

On the other hand, it is worth noting the behavior of the predicted pion form factor in the region $m_{\pi\pi} < 0.5$ GeV down to the negative s region. Figure 15 shows that the pion form factor derived from fits describes quite well the (highly constraining) spacelike data down to about -0.15 GeV². Whether spacelike data are included within the data sample submitted to fit (full curve) or not (dashed curve) does not make any difference (both curves coincide within the thickness of the lines). This is a noticeable property as, following Section 6 in [19], the NA7 data should be rescaled. The rescaling factor $1 - \lambda$ is such that λ depends on the spacelike data, on their scale uncertainties (0.8 % for NA7 [35]) and on the fitting function. Therefore, by ascertaining the threshold behavior of the pion form factor, Figure 15 proves that the contribution of the $\pi\pi$ threshold region to $g - 2$ predicted using the NSK and KLOE10 data

²⁹One may remark that the pion form factor fitting function used in [34] does not include a ϕ term.

is reliable and confirmed by the existing spacelike data. Indeed, these are well accounted for without any regard to their being included within the data sample submitted to fit (see Figure (15c)).

Anyway, the statistical significance of Δa_μ for the preferred solution is 4.88σ . On the other hand, Figure 14 has shown that using or not the τ spectra does not significantly modify the significance for Δa_μ ($5.0\sigma \rightarrow 4.9\sigma$). In contrast, Figure 14 also shows that using the KLOE10 data sample increases the significance by about 0.5σ .

In view of all these considerations, especially the issues encountered with the ϕ region physics information, the most reliable estimate we can propose is :

$$\left\{ \begin{array}{l} a_\mu^{th} = (11\,659\,169.55 + \left[\begin{smallmatrix} +1.26 \\ -0.59 \end{smallmatrix} \right]_\phi \pm 5.21_{th}) 10^{-10} , \\ \Delta a_\mu = a_\mu^{exp} - a_\mu^{th} = (39.35 + \left[\begin{smallmatrix} +0.59 \\ -1.26 \end{smallmatrix} \right]_\phi \pm 5.23_{th} \pm 6.3_{exp}) 10^{-10} , \\ a_\mu^{LO-HVP} = (681.82 + \left[\begin{smallmatrix} +1.26 \\ -0.59 \end{smallmatrix} \right]_\phi \pm 4.51_{th}) 10^{-10} . \end{array} \right. \quad (14)$$

The quoted $[\delta a_\mu^{th}]_\phi$ is an estimate of the possible uncertainties affecting the ϕ region and emphasized in Subsection 5.1.4 and also just above; the central value is derived from a fit within configuration B and avoiding the use the SND phase constraint. $[\delta a_\mu^{th}]_\phi$ should not be added in quadrature to the theoretical error but linearly to the central value. Accounting for this possible shift slightly lessens the significance for Δa_μ from $4.81\sigma \rightarrow 4.67\sigma$.

Therefore, Figure 14 illustrates that the global fit approach allows for a gain in the significance for Δa_μ of about 1σ or more compared to the traditional methods based on numerical integration of the experimental cross sections [8, 6, 7, 9]. It has also been shown that the central value for a_μ^{th} coincides almost exactly with its τ +PDG prediction. Moreover, our approach has allowed us to define the largest set of data samples which exhibit full consistency with each other.

The results involving the fit of the scan \oplus (all/selected) ISR data, do not lead to a noticeably smaller uncertainty for Δa_μ compared to using only scan data, as already inferred in [13]. Indeed, Figure 14 indicates that in changing the fit conditions $[\text{scan} \oplus \tau] \rightarrow [\text{scan} \oplus \tau \oplus \text{KLOE10}]$, the uncertainty marginally improves ($5.28 \rightarrow 5.21$), while the central value moves by 3 units ($36.88 \rightarrow 39.91$), increasing the significance ($4.5\sigma \rightarrow 4.9\sigma$).

7 Conclusion and Perspectives

The $e^+e^- \rightarrow \pi^+\pi^-$ annihilation channel has been widely studied and one is faced with several data sets collected by different groups under various conditions. Beside the scan experiments performed by the CMD-2 and SND collaborations which have produced valuable data samples [26, 27, 28, 29], experiments using the Initial State Radiation (ISR) method have also been performed by the KLOE and BaBar collaborations and have produced (much) higher statistics data samples [31, 32, 33]. The noticeable gain in statistics – for what concerns the $\pi^+\pi^-$ intermediate state – is partly balanced by the issues raised by the dominance of systematic uncertainties. Indeed, comparing the properties of these data samples reveals inconsistencies which leads to somewhat contradictory conclusions concerning the predicted value for the muon anomalous moment.

It thus becomes a relevant challenge to find a tool able to examine critically the properties of the various available samples and substantiate their differences. The present study has proved that the existing data for :

- The e^+e^- annihilation to the $\pi^0\gamma, \eta\gamma, \pi^+\pi^-\pi^0, K^+K^-, K^0\bar{K}^0$ final states,
- The dipion spectra in the $\tau^\pm \rightarrow \pi^\pm\pi^0\nu$ decay,
- Some radiative decays (namely, $\pi^0/\eta/\eta' \rightarrow \gamma\gamma, \rho^\pm \rightarrow \pi^\pm\gamma, K^* \rightarrow K\gamma, \eta' \rightarrow \omega\gamma, \phi \rightarrow \eta'\gamma$) as given in the RPP,

supplemented with some limited isospin breaking (IB) information, provide a benchmark able to reconstruct with a noticeable precision the pion form factor measured in the $e^+e^- \rightarrow \pi^+\pi^-$ annihilation. As could have been expected, the requested IB pieces should cover the $\omega/\phi \rightarrow \pi^+\pi^-$ decays, but also the $\rho^0 \rightarrow e^+e^-$ decay, rarely stressed explicitly [7].

The tool for this prediction is the broken HLS model (BHLS) defined and studied in [13]. In this last reference, the scan data for the $e^+e^- \rightarrow \pi^+\pi^-$ annihilation channel were used. However, the present study has proved that replacing these data by only the $\rho^0/\omega/\phi$ decay data just referred to, allows BHLS to pin down all the parameters of the model and provide strikingly precise predictions for $e^+e^- \rightarrow \pi^+\pi^-$. These have been named "τ+PDG" predictions of the pion form factor. As these predictions are clearly a new way to formulate τ based predictions for the HVP, BHLS provides also a new tool to explore the long reported τ versus e^+e^- discrepancy between the HVP evaluations.

Then, the present study leads to the following conclusions :

- **1/** There is no mismatch between τ based predictions and direct e^+e^- evaluation of the HVP if one relies on BHLS and, especially, on its isospin breaking scheme. This is essentially implemented in two steps : direct breaking at the HLS Lagrangian level followed by vector meson mixing. The vector meson mixing, which generates physical vector fields, is unavoidable because, at first order in breaking parameters, the ideal vector fields are no longer mass eigenstates. This simply confirms the study in [13].
- **2/** The τ +PDG predictions compare astonishingly to the KLOE data samples all along the spectra. Because of their influence on the PDG information, it is somewhat paradoxical to observe a difference between the NSK data and the τ +PDG predictions, more marked than with both KLOE data samples. However, a 1σ modification of the width for $\omega \rightarrow \pi^+\pi^-$ allows to recover a good agreement between the NSK data and the τ +PDG predictions. In contrast, the predicted pion form factor reveals an important disagreement with BaBar data, especially in the $[0.74, 0.78]$ GeV region.
- **3/** By varying the fit conditions, it has been found that the KLOE10 and the scan (NSK) data samples together lead to global fits with outstanding statistical properties. Even if the KLOE08 data sample has properties similar to KLOE10 (see Figures 9 and 8), it looks premature to include it within the global fit procedure³⁰.

³⁰An extraction of the pion form factor from the KLOE 2008 data is presently under way, which relies on using the $\pi\pi\gamma/\mu\mu\gamma$ event ratio [51]. As this implies a dealing with uncertainties slightly different from [31], this might change the picture.

From our analysis, one also gets :

$$F_\omega \equiv \text{Br}(\omega \rightarrow e^+e^-) \times \text{Br}(\omega \rightarrow \pi^+\pi^-) = (1.166 \pm 0.036) 10^{-6} ,$$

close to the presently accepted [24] value and twice more precise, with a corresponding Orsay phase of $104.73^\circ \pm 0.63^\circ$. This value is in accord with the values derived from separate fits to scan, KLOE10 and KLOE08 data samples, reflecting that the lineshape of their pion form factors are consistent with each other. In contrast, the F_ω value derived from (global) fit to the BaBar data sample is different by about $(7 \div 8)\sigma$.

Concerning the ϕ meson region, our analysis of BaBar data provides $\text{Br}(\phi \rightarrow e^+e^-) \times \text{Br}(\phi \rightarrow \pi^+\pi^-) = (3.31 \pm 0.99) 10^{-8}$ in good agreement with the accepted value [24]. The corresponding Orsay phase, however, seems to disagree with expectations [48]; our fits tend to favor $-48.23^\circ \pm 1.88^\circ$, closer to the SND phase.

Using the KLOE10 and the scan data samples leads to the most probable value for the muon anomalous moment :

$$a_\mu^{th} = (11\,659\,169.55 + \left[\begin{smallmatrix} +1.26 \\ -0.59 \end{smallmatrix} \right]_\phi \pm 5.21_{th}) 10^{-10} ,$$

which exhibits a significance for $\Delta a_\mu = a_\mu^{exp} - a_\mu^{th}$ at a $(4.7 \div 4.9)\sigma$ level, significantly larger than the results fully derived by direct numerical integration of the experimental cross sections.

Some additional remarks are worth being made concerning this result and our approach :

- **4/** The cross sections which should be integrated within the BHLS model to evaluate a_μ^{th} can be considered as an "effective field theory induced interpolation" between data points. By using a relatively fine energy binning, the interpolation uncertainties are certainly minimized in all regions, and for all cross sections, which exhibit sharp energy variations. This is certainly an advantage over the standard method which should rely on trapezoidal estimation between relatively distant measured data points, possibly improved by taking somewhat into account the local curvatures.
- **5/** One has certainly noted that the value for a_μ^{th} we privilege is smaller than all estimates involving *all* ISR data. As explained above, this is because the effects of the KLOE sample is not balanced by the BaBar data. However, as noted several times above, the value for F_ω is a criterion which leads us to conclude that NSK and KLOE10 only have homogeneous properties which justify to privilege a global simultaneous fit of these.
- **6/** The poor description of the BaBar data within the global fit framework does not mean that it cannot yield a good description in a really standalone fit. However, the global fit method, which accounts for the underlying physics correlations, performs quite successfully with other data samples covering the same physics and the same energy region. As, it is unlikely that BHLS may have some inherent reason to exhibit some tropism towards the scan or KLOE data, we indeed consider the a_μ^{th} value we propose as the most motivated one on statistical grounds. Of course, new ISR data one can expect from Belle are clearly valuable.

Nevertheless, the results derived using all $\pi^+\pi^-$ ISR data samples have been examined (see Figure 13) and shown to agree with the favored estimate just quoted. Because of the properties expected from the (BHLS) global framework recalled in the Introduction, using only the KLOE10 and NSK data samples provides already as precise results as those derived using all available ISR data samples and the traditional evaluation method of a_μ^{LO-HVP} .

Our work tells that the significance for Δa_μ starts to be close to the 5σ level. How close to this value it could be, should be confirmed by more precise annihilation data in the $[0.95, 1.05]$ GeV mass region, especially in the $\pi^+\pi^-$, $\pi^+\pi^-\pi^0$ final states. Finally, new measurements for the experimental value of the muon $g - 2$ are planned [52, 53]; they are important so as to confirm the central value for a_μ^{exp} , and also to lessen the experimental uncertainty which starts now to be dominant when estimating the significance for Δa_μ .

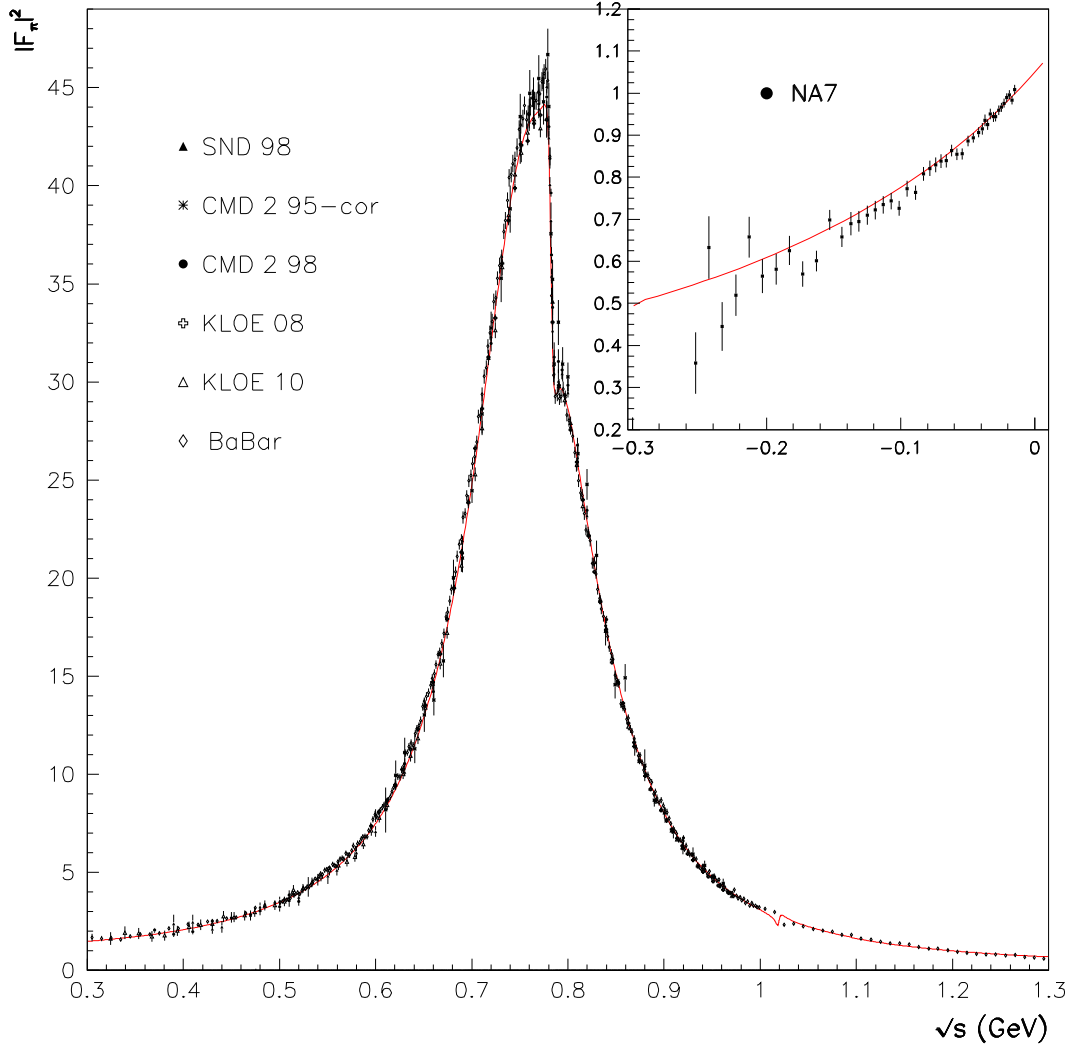


Figure 2: The Pion Form Factor *prediction* based on τ data and PDG information. The most important experimental data are superimposed; they do not influence the predicted curve.

References

- [1] T. Aoyama, M. Hayakawa, T. Kinoshita, and M. Nio, (2012), 1205.5368, Tenth-Order QED Contribution to the Electron $g-2$ and an Improved Value of the Fine Structure Constant.
- [2] T. Aoyama, M. Hayakawa, T. Kinoshita, and M. Nio, (2012), 1205.5370, Complete Tenth-Order QED Contribution to the Muon $g-2$.

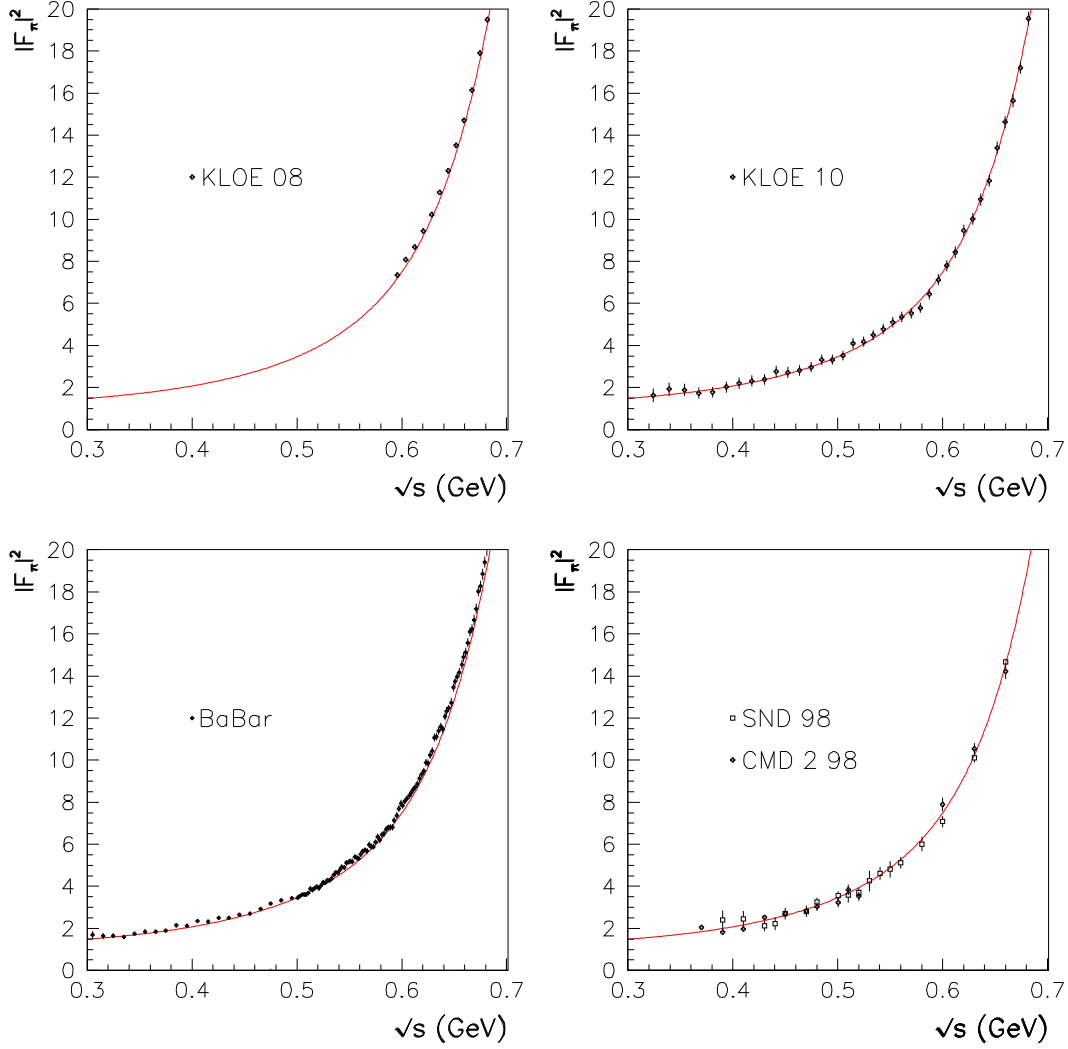


Figure 3: Magnified view of the Pion Form Factor *prediction* based on τ data and PDG information; the $(0.3 \div 0.7)$ GeV region is shown with the indicated data superimposed.

- [3] M. Passera, Phys.Rev. **D75**, 013002 (2007), hep-ph/0606174, Precise mass-dependent QED contributions to leptonic g-2 at order α^2 and α^3 .
- [4] F. Jegerlehner and A. Nyffeler, Phys. Rept. **477**, 1 (2009), 0902.3360, The Muon g-2.
- [5] J. Prades, E. de Rafael, and A. Vainshtein, (2009), 0901.0306, Hadronic Light-by-Light Scattering Contribution to the Muon Anomalous Magnetic Moment.

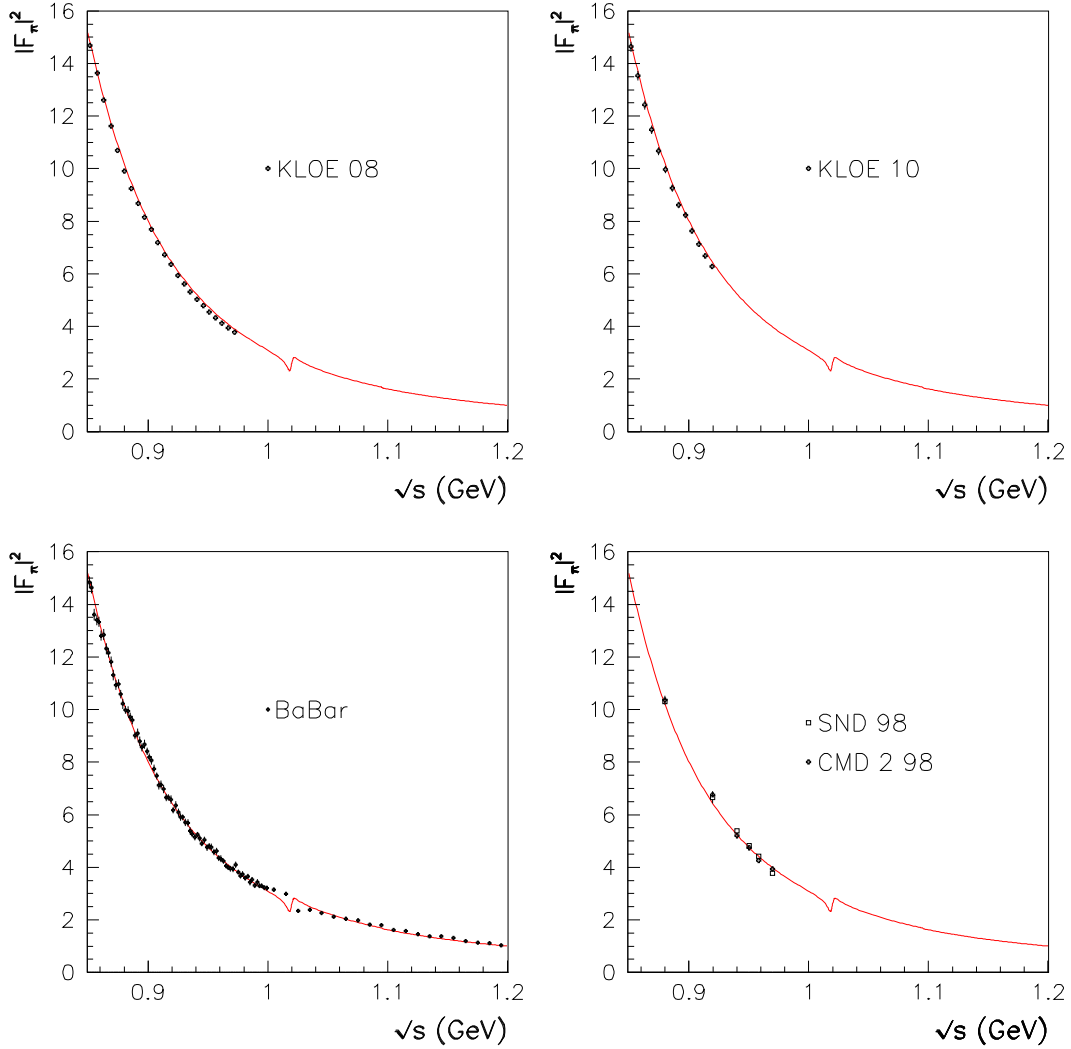


Figure 4: Magnified view of the Pion Form Factor *prediction* based on τ data and PDG information; the $(0.85 \div 1.2)$ GeV region is shown with the indicated data superimposed.

- [6] M. Davier, A. Hoecker, B. Malaescu, and Z. Zhang, Eur. Phys. J. **C71**, 1515 (2011), 1010.4180, Reevaluation of the Hadronic Contributions to the Muon $g-2$ and to $\alpha(MZ)$.
- [7] F. Jegerlehner and R. Szafron, (2011), 1101.2872, $\rho^0 - \gamma$ mixing in the neutral channel pion form factor $|F_\pi|^2$ and its role in comparing e^+e^- with τ spectral functions.
- [8] M. Davier *et al.*, Eur. Phys. J. **C66**, 127 (2010), 0906.5443, The Discrepancy Between τ and e^+e^- Spectral Functions Revisited and the Consequences for the Muon Magnetic

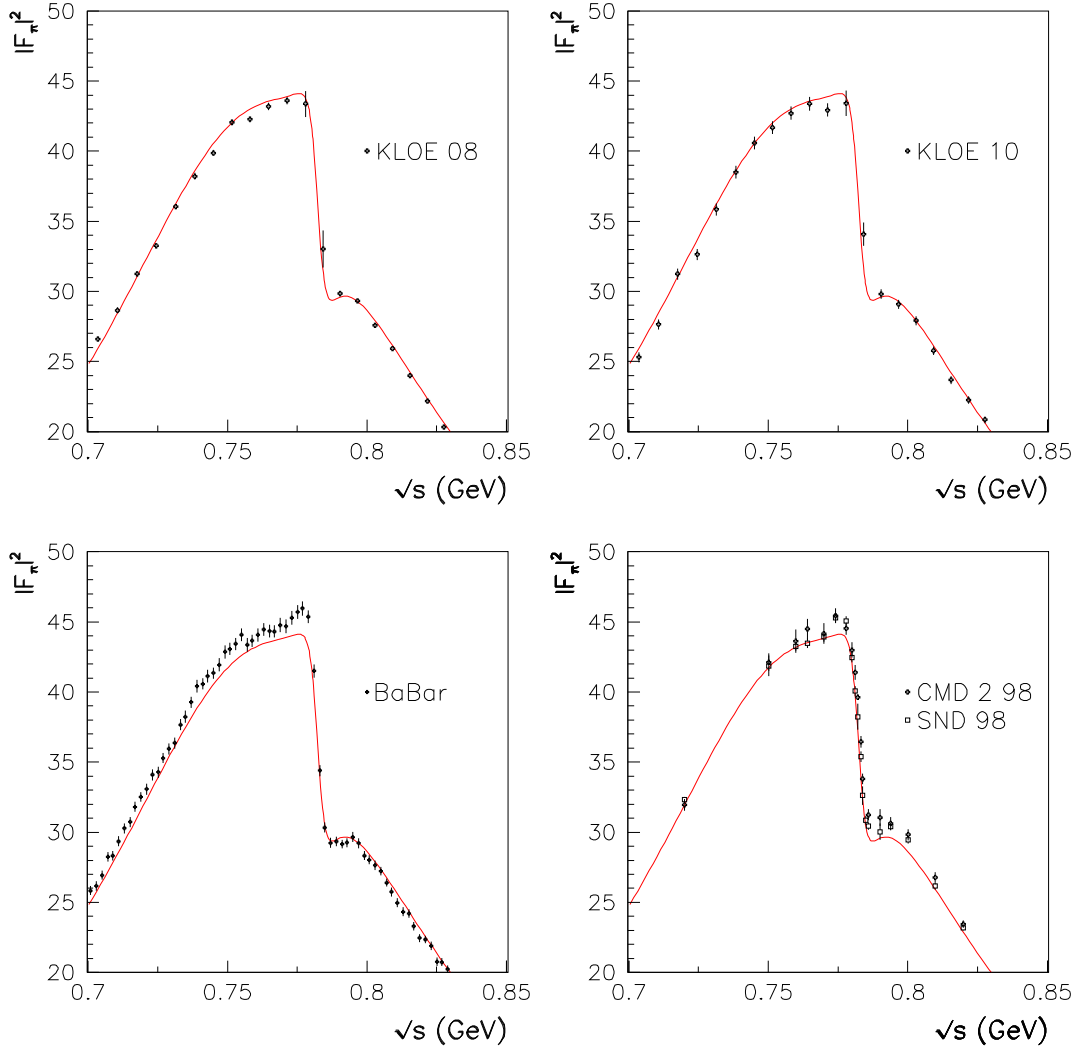


Figure 5: Magnified view of the Pion Form Factor *prediction* based on τ data and PDG information; the $(0.7 \div 0.85)$ GeV region is shown with the indicated data superimposed.

Anomaly.

- [9] K. Hagiwara, R. Liao, A. D. Martin, D. Nomura, and T. Teubner, J.Phys. **G38**, 085003 (2011), 1105.3149, $(g - 2)_\mu$ and $\alpha(M_Z^2)$ re-evaluated using new precise data.
- [10] G. Ecker, J. Gasser, A. Pich, and E. de Rafael, Nucl.Phys. **B321**, 311 (1989), The Role of Resonances in Chiral Perturbation Theory.

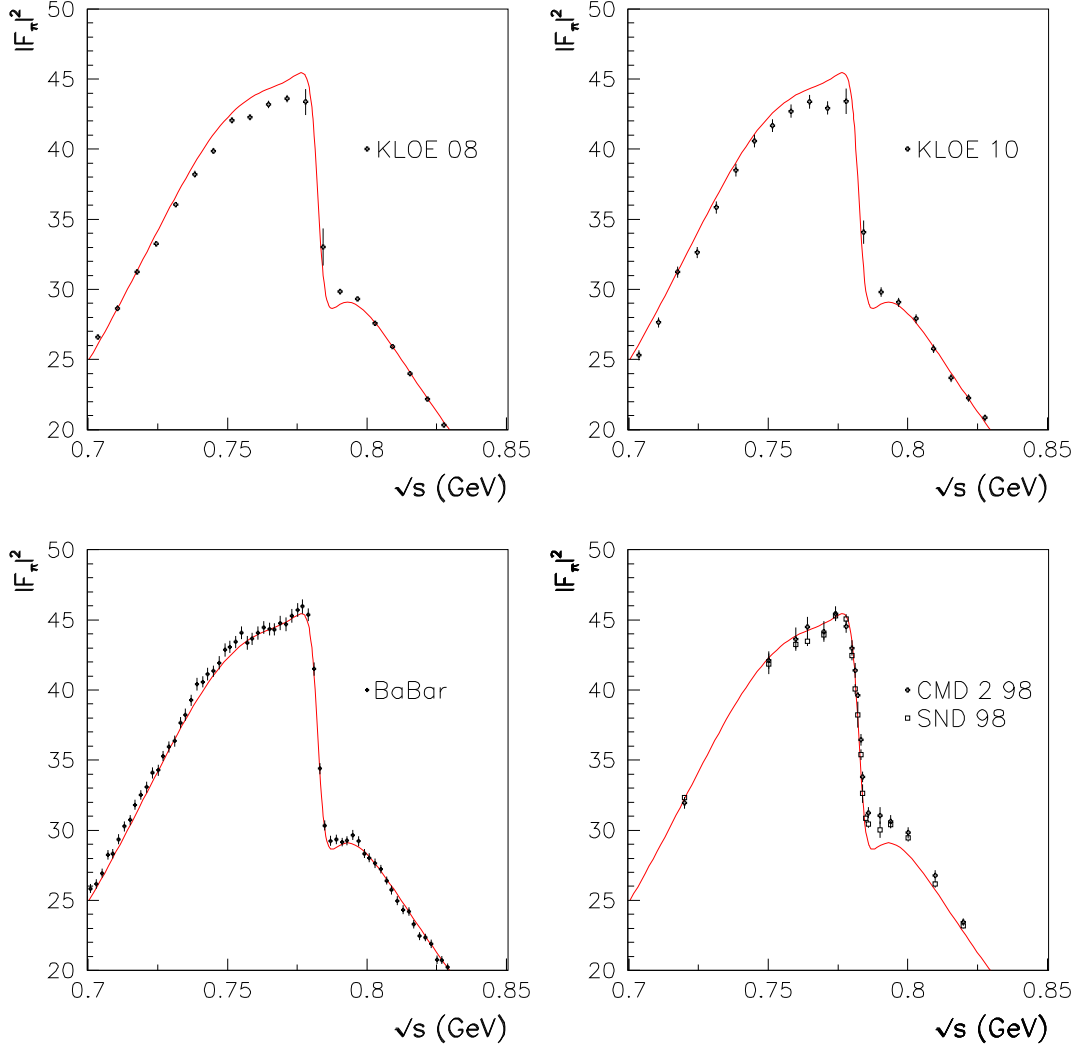


Figure 6: The Pion Form Factor *prediction* based on τ data and the $(0.76 \div 0.82)$ GeV region of the BaBar spectrum [33]; the $(0.7 \div 0.85)$ GeV region is shown with the indicated data superimposed.

- [11] J. Prades, Z. Phys. **C63**, 491 (1994), hep-ph/9302246, Massive spin 1 field chiral Lagrangian from an extended Nambu-Jona-Lasinio model of QCD.
- [12] G. Ecker, J. Gasser, H. Leutwyler, A. Pich, and E. de Rafael, Phys.Lett. **B223**, 425 (1989), Chiral Lagrangians for Massive Spin 1 Fields.
- [13] M. Benayoun, P. David, L. DelBuono, and F. Jegerlehner, Eur.Phys.J. **C72**, 1848 (2012), 1106.1315, Upgraded Breaking Of The HLS Model: A Full Solution to the $\tau^- \rightarrow e^+ e^-$

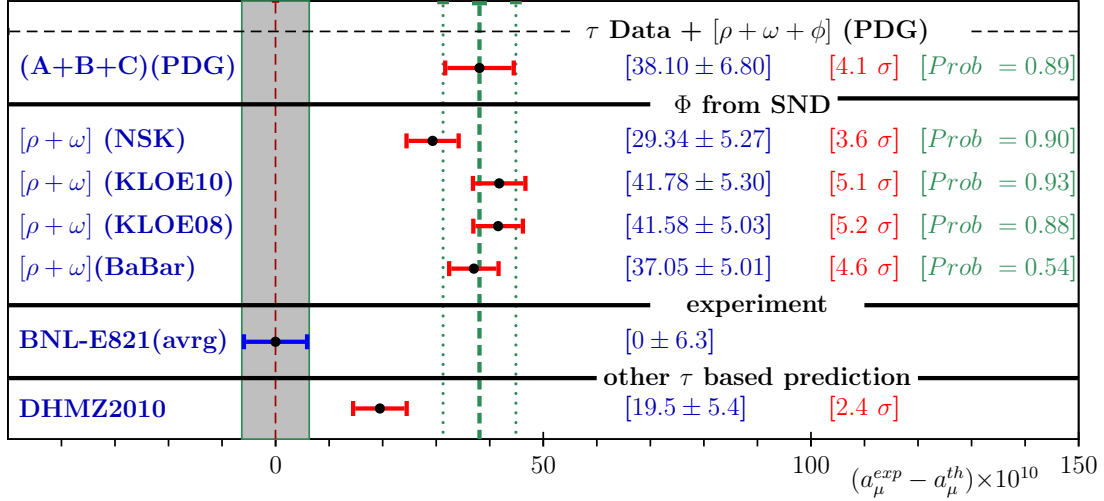


Figure 7: τ based estimates using a global fit of the BHLS model (see Section 4). The first two numbers in each line display resp. the central value and the r.m.s. of $\Delta a_\mu = a_\mu^{exp} - a_\mu^{th}$. The last two numbers give resp. the distance to the BNL measurement and the fit probability – essentially dominated by the non $\pi^+\pi^-$ data. The lower probability found when using the BaBar data, even in the limited energy region involved ($[0.76 \div 0.82]$ GeV), exhibits the tension of this data sample relative to the rest of the physics considered.

and ϕ Decay Issues And Its Consequences On g-2 VMD Estimates.

- [14] M. Bando, T. Kugo, and K. Yamawaki, Phys. Rept. **164**, 217 (1988), Nonlinear Realization and Hidden Local Symmetries.
- [15] M. Harada and K. Yamawaki, Phys. Rept. **381**, 1 (2003), hep-ph/0302103, Hidden local symmetry at loop: A new perspective of composite gauge boson and chiral phase transition.
- [16] M. Bando, T. Kugo, and K. Yamawaki, Nucl. Phys. **B259**, 493 (1985), On the Vector Mesons as Dynamical Gauge Bosons of Hidden Local Symmetries.
- [17] M. Benayoun and H. B. O’Connell, Phys. Rev. **D58**, 074006 (1998), hep-ph/9804391, SU(3) breaking and hidden local symmetry.
- [18] M. Benayoun, P. David, L. DelBuono, O. Leitner, and H. B. O’Connell, Eur. Phys. J. **C55**, 199 (2008), hep-ph/0711.4482, The Dipion Mass Spectrum In e^+e^- Annihilation and tau Decay: A Dynamical (ρ^0, ω, ϕ) Mixing Approach.
- [19] M. Benayoun, P. David, L. DelBuono, and O. Leitner, Eur. Phys. J. **C65**, 211 (2010), 0907.4047, A Global Treatment Of VMD Physics Up To The ϕ : I. e^+e^- Annihilations, Anomalies And Vector Meson Partial Widths.

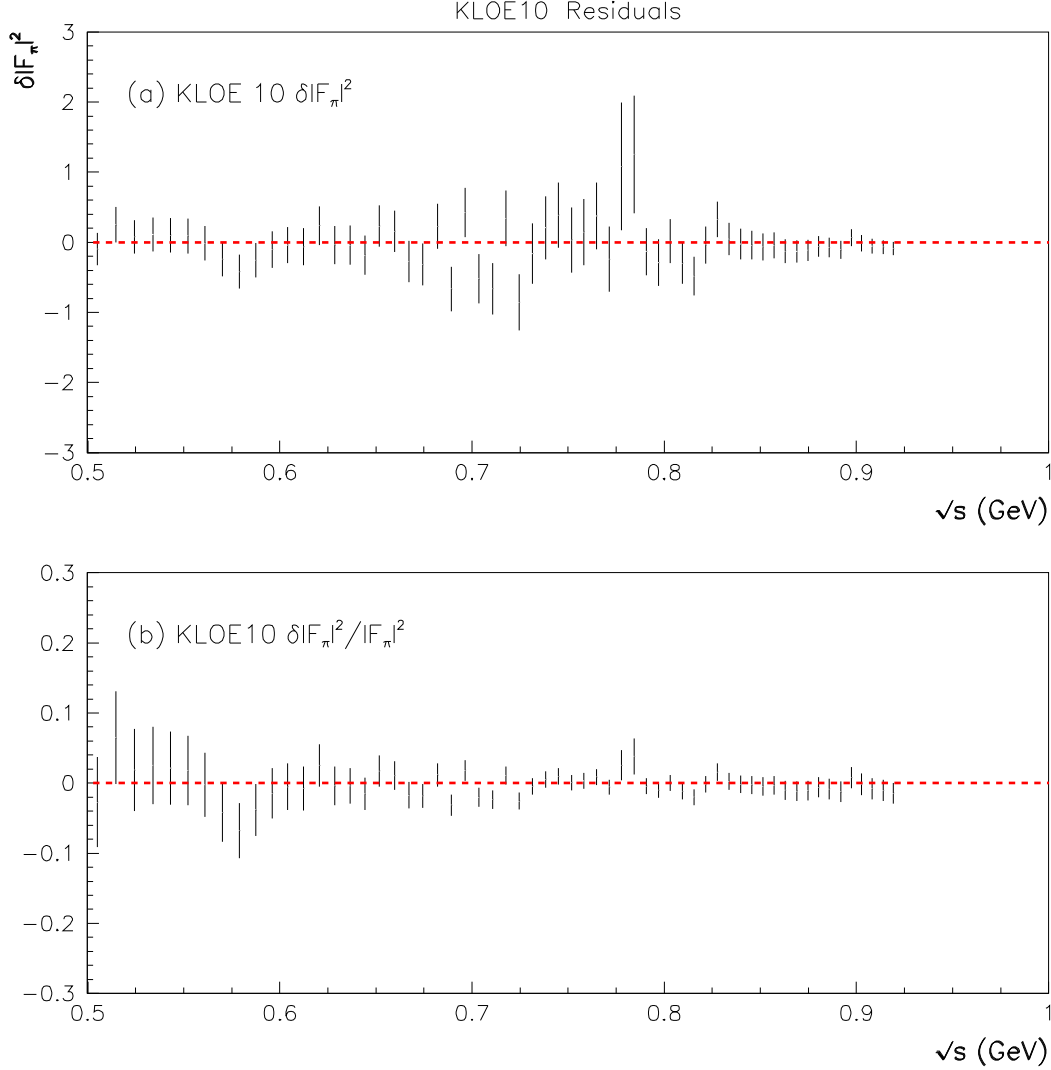


Figure 8: Fit residuals for the KLOE10 data in isolation²³. The top panel shows the function $\delta|F_\pi(s)|^2 = |F_\pi^{KLOE10}(s)|^2 - |F_\pi^{fit}(s)|^2$; the bottom panel displays the distribution $\delta|F_\pi(s)|^2/|F_\pi^{fit}(s)|^2$.

[20] M. Benayoun, P. David, L. DelBuono, and O. Leitner, Eur. Phys. J. **C68**, 355 (2010), 0907.5603, A Global Treatment Of VMD Physics Up To The phi: II. τ Decay and Hadronic Contributions To g-2.

[21] ALEPH, S. Schael *et al.*, Phys. Rept. **421**, 191 (2005), hep-ex/0506072, Branching ratios and spectral functions of tau decays: Final ALEPH measurements and physics implications.

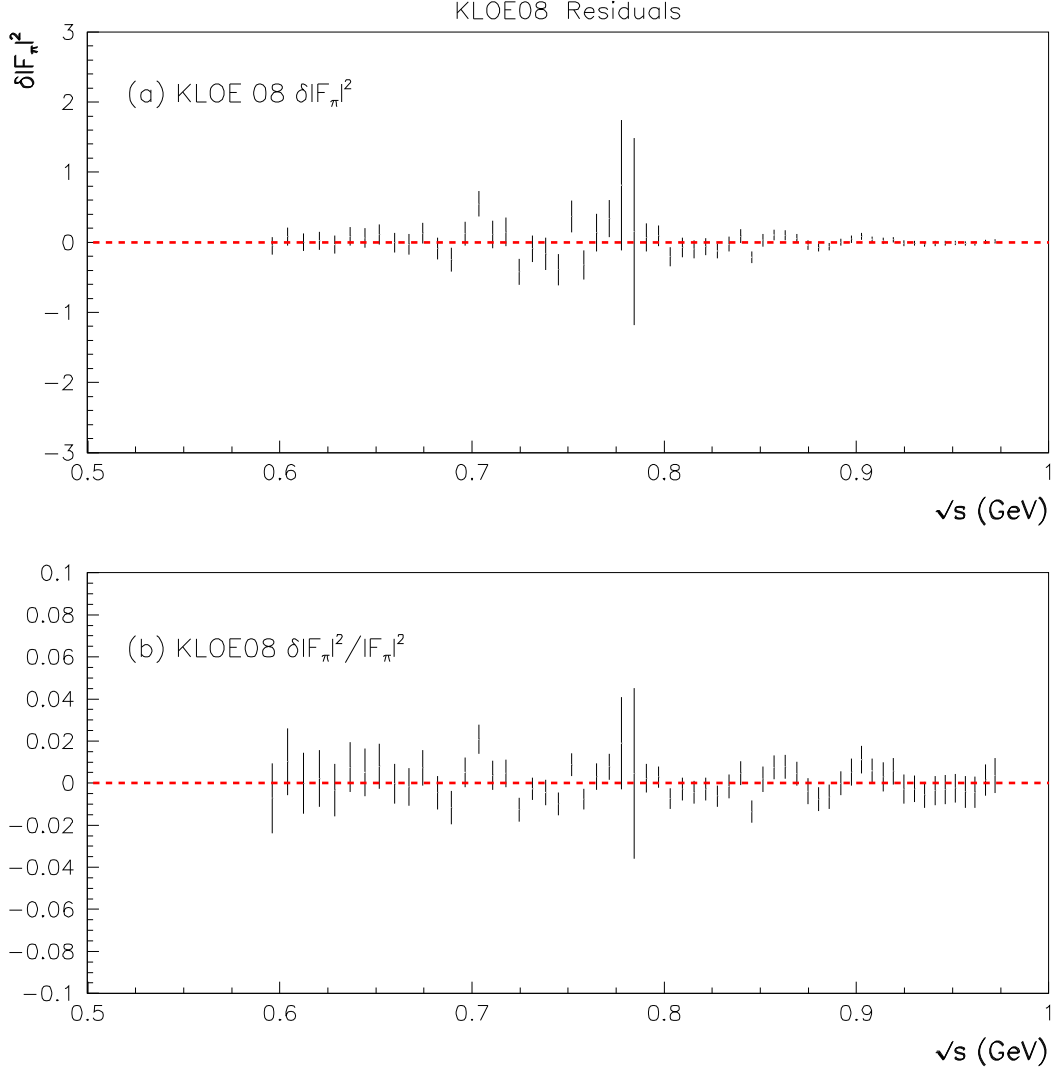


Figure 9: Fit residuals for the KLOE08 data in isolation²³. The top panel shows the function $\delta|F_\pi(s)|^2 = |F_\pi^{KLOE08}(s)|^2 - |F_\pi^{fit}(s)|^2$; the bottom panel displays the distribution $\delta|F_\pi(s)|^2/|F_\pi^{fit}(s)|^2$.

[22] CLEO, S. Anderson *et al.*, Phys. Rev. **D61**, 112002 (2000), hep-ex/9910046, Hadronic structure in the decay $\tau^- \rightarrow \pi^- \pi^0 \nu_\tau$.

[23] Belle, M. Fujikawa *et al.*, Phys. Rev. **D78**, 072006 (2008), 0805.3773, High-Statistics Study of the $\tau^- \rightarrow \pi^- \pi^0 \nu_\tau$ Decay.

[24] Particle Data Group, K. Nakamura *et al.*, J. Phys. **G37**, 075021 (2010), Review of Particle Physics.

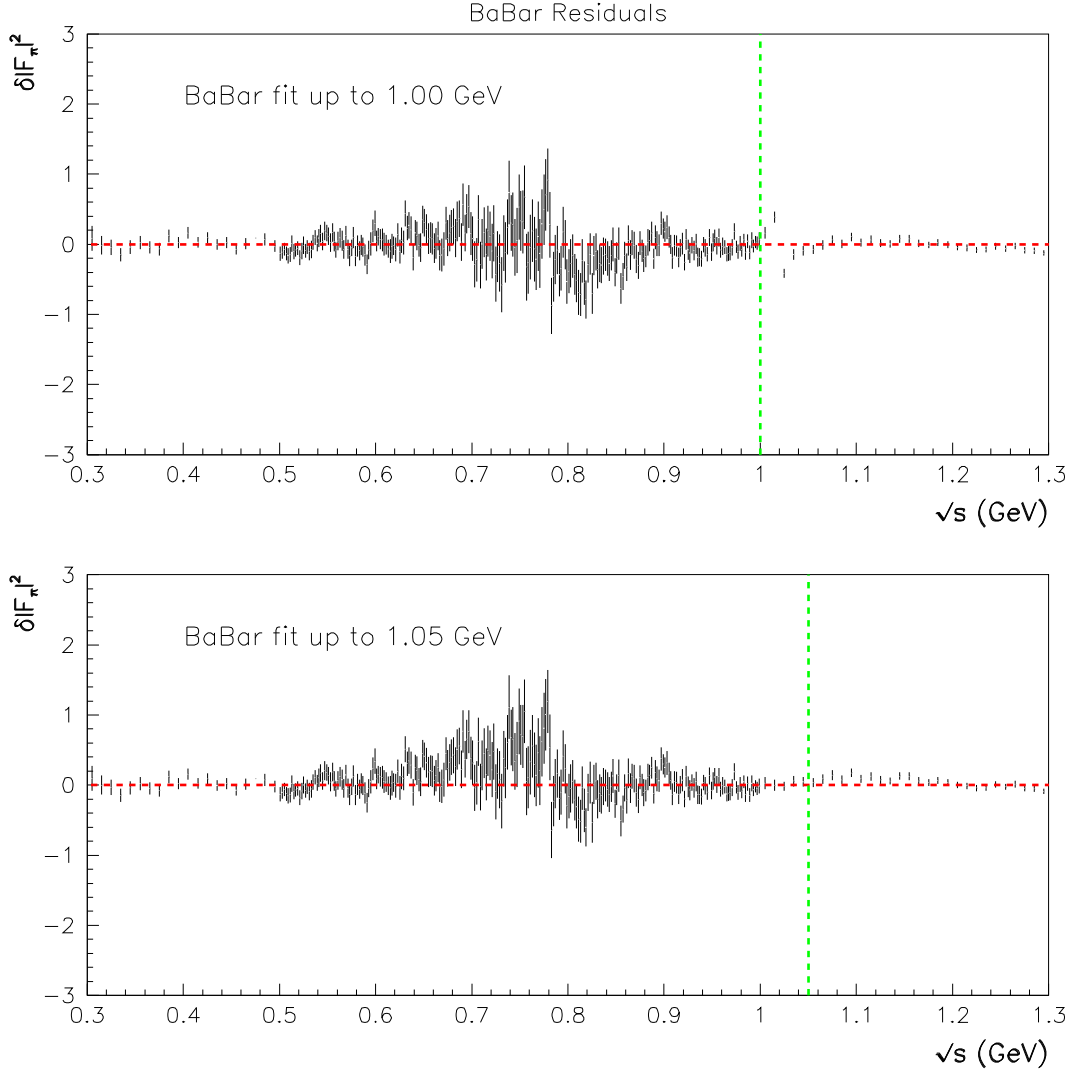


Figure 10: Fit residuals for the BaBar data sample in isolation²³. The top panel shows the residual distribution when fitting only up to 1.0 GeV, the bottom panel shows the residual distribution when the fit is extended up to 1.05 GeV. The vertical dashed lines indicate, in each case, the upper end of the spectrum submitted to fit.

- [25] L. M. Barkov *et al.*, Nucl. Phys. **B256**, 365 (1985), Electromagnetic Pion Form-Factor in the Timelike Region.
- [26] CMD-2, R. R. Akhmetshin *et al.*, Phys. Lett. **B578**, 285 (2004), hep-ex/0308008, Re-analysis of hadronic cross section measurements at CMD- 2.
- [27] CMD-2, R. R. Akhmetshin *et al.*, Phys. Lett. **B648**, 28 (2007), hep-ex/0610021, High-

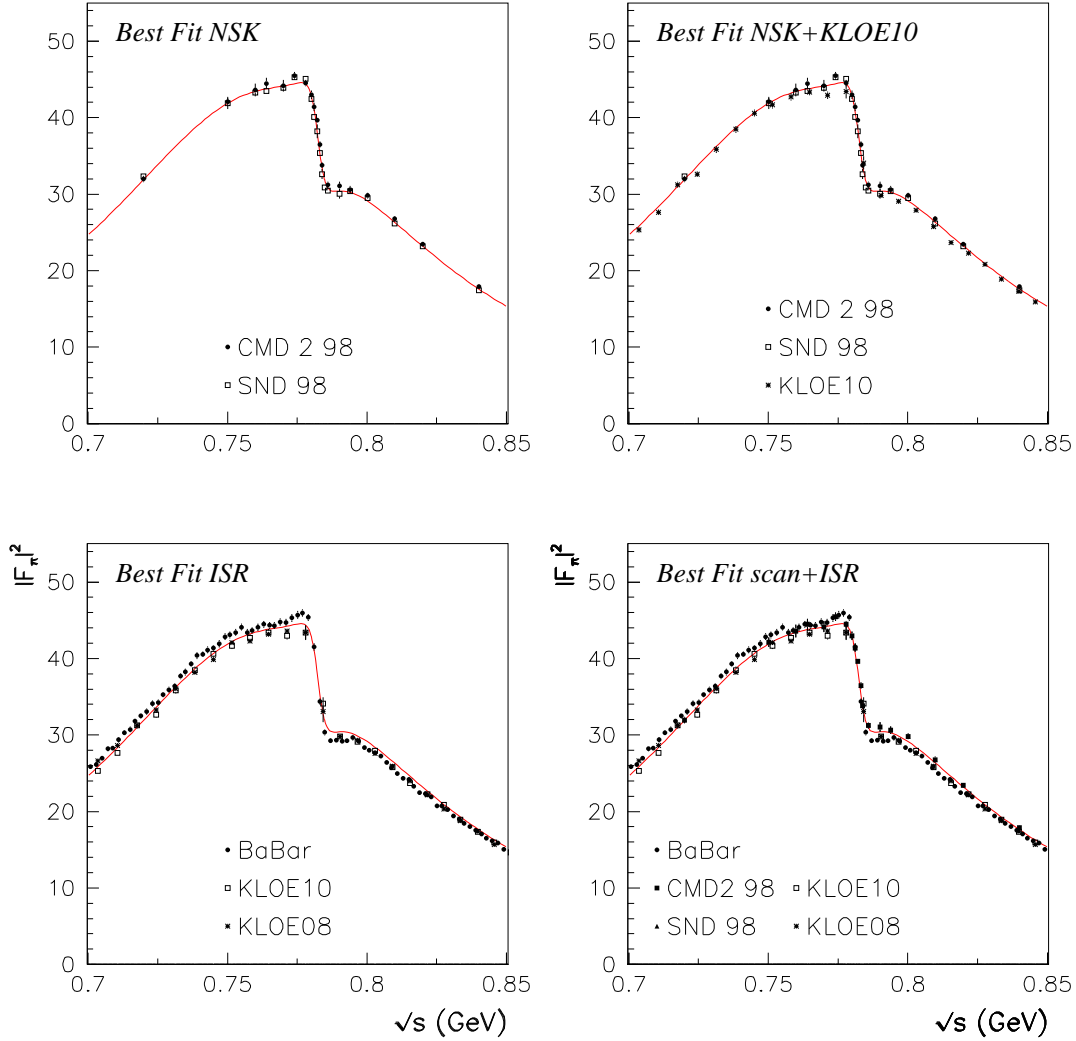


Figure 11: The Pion Form Factor in the $\rho - \omega$ region from various global fit configurations. Top left panel displays the best fit using only the CMD-2 and SND data as $e^+e^- \rightarrow \pi^+\pi^-$ spectra. Top right panel shows the case when the CMD-2, SND and KLOE10 data samples are fitted simultaneously. Bottom left panel shows the best fits when the data samples considered are those from BaBar, KLOE08 and KLOE10. Bottom right panel shows the best fit using simultaneously the CMD-2, SND, KLOE08, KLOE10 and BaBar data samples.

statistics measurement of the pion form factor in the rho-meson energy range with the CMD-2 detector.

- [28] R. R. Akhmetshin *et al.*, JETP Lett. **84**, 413 (2006), hep-ex/0610016, Measurement of the $e^+e^- \rightarrow \pi^+\pi^-$ cross section with the CMD-2 detector in the 370-MeV - 520-MeV

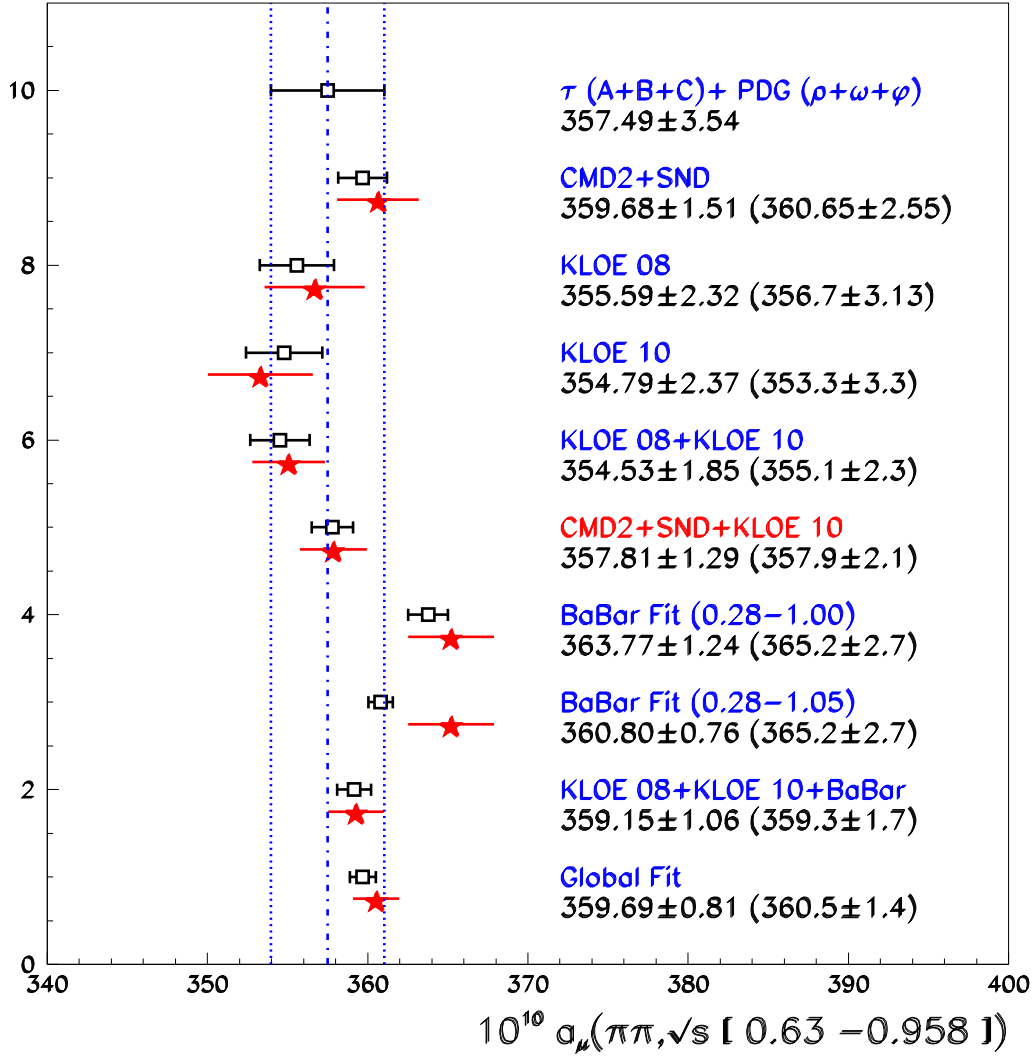


Figure 12: The muon anomalous magnetic moment. The numbers gives the $\pi\pi$ contribution from the (0.630, 0.958) GeV invariant mass region. The results from fits are shown with empty squares, the experimental estimates by stars. Fit values are given followed by the experimental estimate within brackets. Global fit properties favor the result from the CMD2+SND+KLOE10 combined sample.

cm energy range.

- [29] M. N. Achasov *et al.*, J. Exp. Theor. Phys. **103**, 380 (2006), hep-ex/0605013, Update of the $e^+e^- \rightarrow \pi^+\pi^-$ cross section measured by SND detector in the energy region $400\text{-MeV} < \sqrt{s} < 1000\text{-MeV}$.

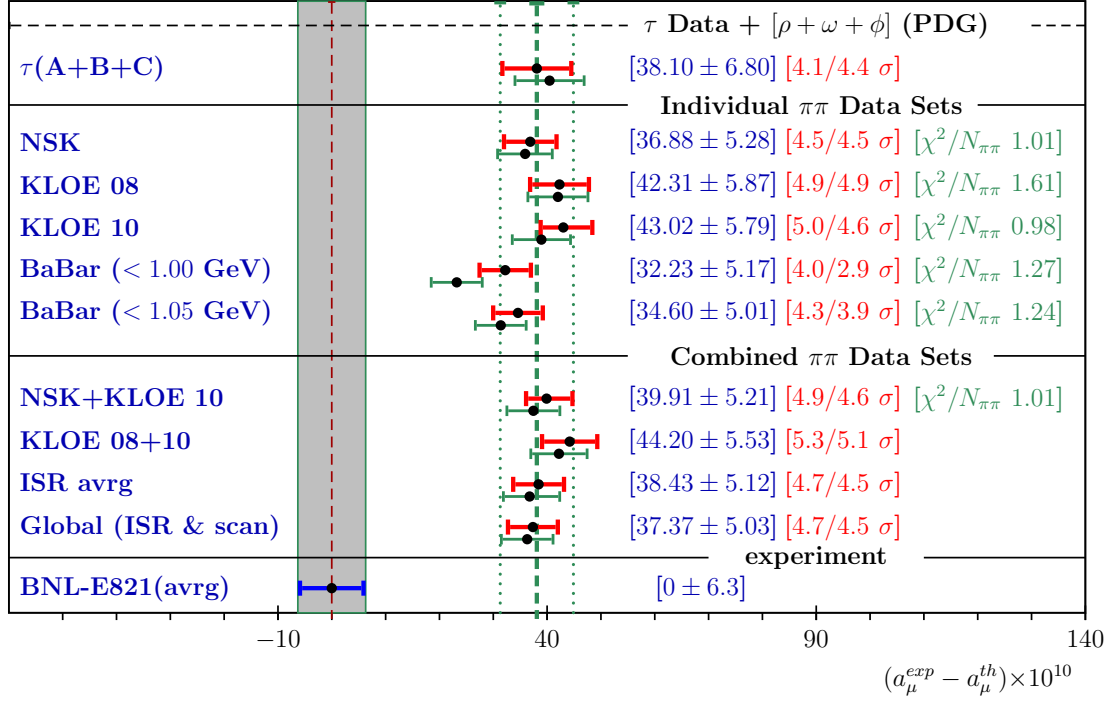


Figure 13: The deviation $\Delta a_\mu \times 10^{10}$ between experiment and theory for the anomalous magnetic moment of the muon. The leading hadronic vacuum polarization contribution has been estimated via global BHLS model fits for different $e^+e^- \rightarrow \pi^+\pi^-$ data samples. The τ predictions – using or not the spacelike data – are given in the top pair lines, followed by the fit results using each scan or ISR data sample in isolation or combined; see text for comments.

- [30] M. Davier, A. Hoecker, B. Malaescu, C. Z. Yuan, and Z. Zhang, (2009), 0908.4300, Reevaluation of the hadronic contribution to the muon magnetic anomaly using new $e^+e^- \rightarrow \pi^+\pi^-$ cross section data from BABAR.
- [31] KLOE, G. Venanzoni *et al.*, (2009), 0906.4331, A precise new KLOE measurement of $|F_\pi|^2$ with ISR events and determination of $\pi\pi$ contribution to a_μ for $0.592 < M_{\pi\pi} < 0.975$ GeV.
- [32] KLOE, F. Ambrosino *et al.*, (2010), 1006.5313, Measurement of $\sigma(e^+e^- \rightarrow \pi^+\pi^-)$ from threshold to 0.85 GeV^2 using Initial State Radiation with the KLOE detector.
- [33] BABAR, B. Aubert *et al.*, Phys. Rev. Lett. **103**, 231801 (2009), 0908.3589, Precise measurement of the $e^+e^- \rightarrow \pi^+\pi^-(\gamma)$ cross section with the Initial State Radiation method at BABAR.
- [34] BABAR Collaboration, J. Lees *et al.*, Phys.Rev. **D86**, 032013 (2012), 1205.2228, Precise Measurement of the $e^+e^- \rightarrow \pi^+\pi^-(\gamma)$ Cross Section with the Initial-State Radiation Method at BABAR.

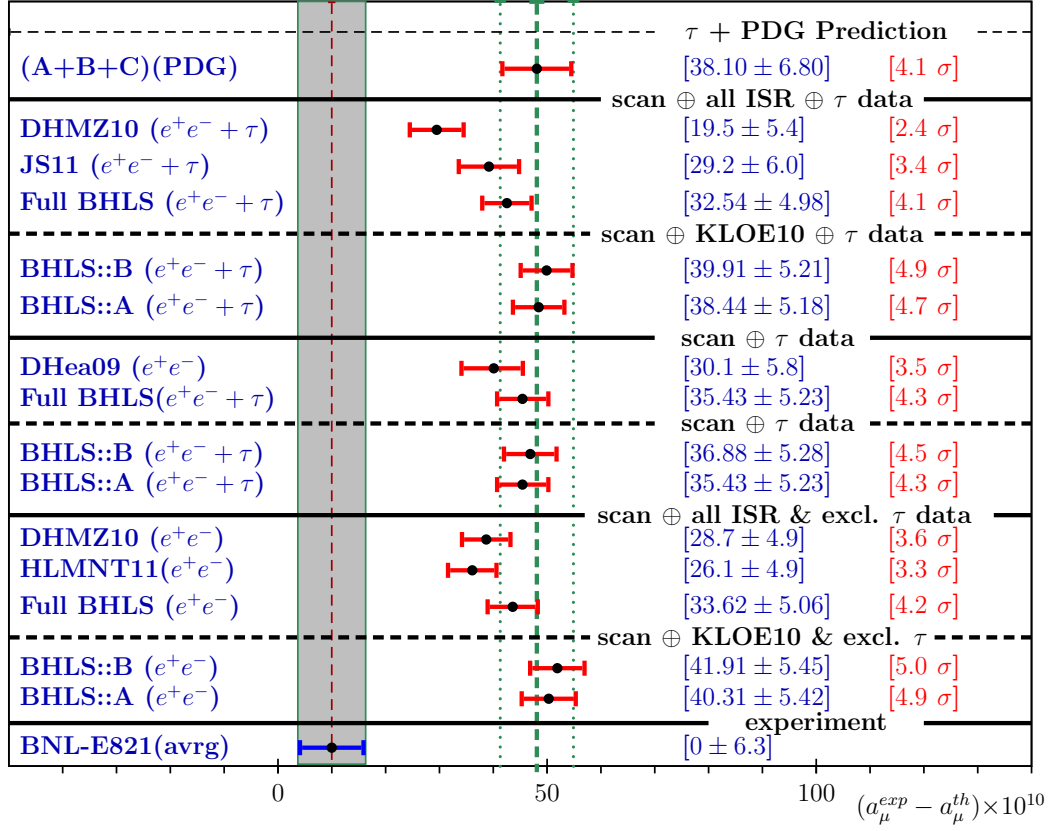


Figure 14: A set of recent estimates of the muon anomalous magnetic moment deviation from the BNL average value [39, 40]. Our own (updated) estimates are figured by BHLS::A and BHLS::B for respectively configurations A and B. The results obtained using *all* the ISR data samples inside the global fit procedure are displayed under the tag Full BHLS. The statistical significance of each Δa_μ is displayed on the right hand side of the Figure. See the text for more information.

- [35] NA7, S. R. Amendolia *et al.*, Nucl. Phys. **B277**, 168 (1986), A Measurement of the Space - Like Pion Electromagnetic Form-Factor.
- [36] E. B. Dally *et al.*, Phys. Rev. Lett. **48**, 375 (1982), Elastic Scattering Measurement of the Negative Pion Radius.
- [37] ATLAS, G. Aad *et al.*, Phys. Lett. **B716**, 1 (2012), 1207.7214, Observation of a new particle in the search for the Standard Model Higgs boson with the ATLAS detector at the LHC.
- [38] CMS, S. Chatrchyan *et al.*, Phys. Lett. **B716**, 30 (2012), 1207.7235, Observation of a new boson at a mass of 125 GeV with the CMS experiment at the LHC.
- [39] Muon G-2, G. W. Bennett *et al.*, Phys. Rev. **D73**, 072003 (2006), hep-ex/0602035, Final report of the muon E821 anomalous magnetic moment measurement at BNL.

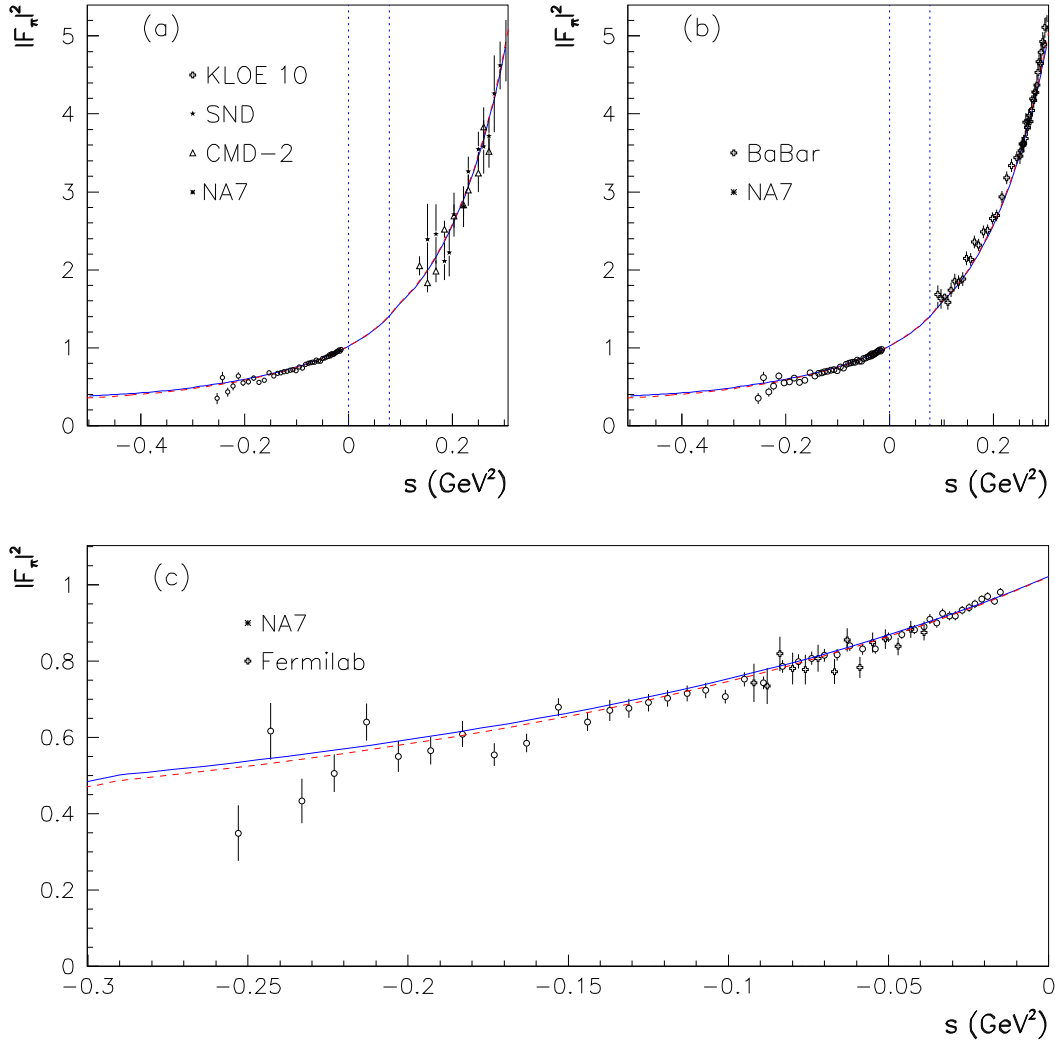


Figure 15: The Pion Form Factor around $s = 0$. The $\pi^+\pi^-$ annihilation data submitted to the global fit are *only* the NSK and KLOE10 samples. The full curve is the fit function derived when including also the spacelike data from NA7 [35] and Fermilab [36]; the dashed curve is associated with the fit excluding the spacelike data. The BaBar data – shown in (b) for illustration – are not submitted to the fit. KLOE08 has no data point located within the plotted window. For clarity, only the data from NA7 [35] are shown in (a) and (b). In (c) One magnifies the spacelike region and plot the data [35, 36], used or not within the fit procedure. The vertical lines in (a) and (b) show the locations $s = 0$ and $s = 4m_\pi^2$.

[40] B. L. Roberts, Chin. Phys. **C34**, 741 (2010), 1001.2898, Status of the Fermilab Muon $(g - 2)$ Experiment.

- [41] J. Gasser and H. Leutwyler, *Annals Phys.* **158**, 142 (1984), Chiral Perturbation Theory to One Loop.
- [42] J. Gasser and H. Leutwyler, *Nucl. Phys.* **B250**, 465 (1985), Chiral Perturbation Theory: Expansions in the Mass of the Strange Quark.
- [43] M. Hashimoto, *Phys. Rev.* **D54**, 5611 (1996), hep-ph/9605422, Hidden local symmetry for anomalous processes with isospin/SU(3) breaking effects.
- [44] G. 't Hooft, *Phys. Rept.* **142**, 357 (1986), How Instantons Solve the U(1) Problem.
- [45] T. Fujiwara, T. Kugo, H. Terao, S. Uehara, and K. Yamawaki, *Prog. Theor. Phys.* **73**, 926 (1985), Nonabelian Anomaly and Vector Mesons as Dynamical Gauge Bosons of Hidden Local Symmetries.
- [46] M. Benayoun *et al.*, *Eur. Phys. J.* **C2**, 269 (1998), hep-ph/9707509, New results in ρ^0 meson physics.
- [47] C. E. Wolfe and K. Maltman, *Phys. Rev.* **D80**, 114024 (2009), 0908.2391, Models of Isospin Breaking in the Pion Form Factor: Consequences for the Determination of $\Pi_{\rho\omega}(m_\rho^2)$ and $(g-2)_\mu/2$.
- [48] M. N. Achasov *et al.*, *Phys. Lett.* **B474**, 188 (2000), hep-ex/0001048, Decay $\phi \rightarrow \pi^+\pi^-$.
- [49] M. Benayoun, www2.fz-juelich.de/ikp//mesonnet/2012_ff_workshop/venue.shtml, Confronting the scan, ISR and tau dipion spectra within a global model.
- [50] P. J. Mohr, B. N. Taylor, and D. B. Newell, (2012), 1203.5425, CODATA Recommended Values of the Fundamental Physical Constants: 2010.
- [51] KLOE/KLOE-2 Collaborations, G. Venanzoni, *Proceedings of the EPS-HEP2011 Conference, Grenoble*, 376 (2011).
- [52] Fermilab P989 Collaboration, B. Lee Roberts, *Nucl.Phys.Proc.Suppl.* **218**, 237 (2011), The Fermilab muon (g-2) project.
- [53] J-PARC New g-2/EDM experiment Collaboration, H. Iinuma, *J.Phys.Conf.Ser.* **295**, 012032 (2011), New approach to the muon g-2 and EDM experiment at J-PARC.